Title:

Evidence for extreme floods in arid subtropical northwest Australia during the Little Ice Age Chronozone (CE 1400–1850)

Authors

A. Rouillard*[a1], G. Skrzypek[a], C. Turney[b], S. Dogramaci[a,c], Q. Hua[d], A. Zawadzki[d], J. Reeves[e], P. Greenwood[a,f,g], A.J. O'Donnell[a] and P.F. Grierson[a]

[a]Ecosystems Research Group and West Australian Biogeochemistry Centre, School of Plant Biology, The University of Western Australia, Crawley, WA 6009, Australia

[b]Climate Change Research Centre, School of Biological, Earth and Environmental Sciences, University of New South Wales, Sydney, NSW 2052, Australia

[c]Rio Tinto Iron Ore, Perth, WA 6000, Australia

[d]Australian Nuclear Science and Technology Organisation (ANSTO), Locked Bag 2001, Kirrawee DC, NSW 2232, Australia

[e]Faculty of Science and Technology, Federation University Australia, PO Box 663, Ballarat VIC 3353, Australia

[f]Centre for Exploration Targeting, School of Earth and Environment, The University of Western Australia, Crawley, WA, Australia

[g]Western Australia Organic and Isotope Geochemistry Centre, The Institute for Geoscience Research, Department of Chemistry, Curtin University, Bentley, WA, Australia

*author for correspondence: alexandra.rouillard@research.uwa.edu.au;
alexandrarouillard@yahoo.ca

[1] Present email and address: alexandra.rouillard@snm.ku.dk; Centre for GeoGenetics, Natural History Museum of Denmark, University of Copenhagen, Øster Voldgade 5-7, 1350 Copenhagen K, Denmark

Abbreviations: Common Era (CE); Constant Initial Concentration (CIC); Constant Rate of Supply (CRS); El Niño-Southern Oscillation (ENSO); Indonesian Australian Summer Monsoon (IASM); Inorganic Carbon (IC); Intertropical Convergence Zone (ITCZ); Little Ice Age (LIA); Madden-Julian/Intra-seasonal Oscillation (MJO); Northern Hemisphere (NH); Organic Carbon (OC); Organic Matter (OM); Southern Annular Mode (SAM); Southern Hemisphere (SH); Tropical Cyclone (TC).

Key words

Hydroclimate, Intertropical Convergence Zone (ITCZ), Late Holocene, Little Ice Age (LIA), Sediment, Paleolimnology, Pilbara

Abstract

Here we report a ~2000-year sediment sequence from the Fortescue Marsh (*Martuyitha*) in the eastern Pilbara region, which we have used to investigate changing hydroclimatic conditions in the arid subtropics of northwest Australia. The Pilbara is located at the intersection of the tropical Indian and Pacific Oceans and its modern rainfall regime is strongly influenced by tropical cyclones, the Intertropical Convergence Zone (ITCZ) and the Indo-Pacific Warm Pool. We identified four distinct periods within from the record. The most recent period (P1: CE ~1990–present) reveals hydroclimatic conditions over recent decades that are the most persistently wet of potentially the last ~2000 years. During the previous centuries (P2: ~CE 1600–1990), the Fortescue Marsh was overall drier but likely punctuated by a number of extreme floods, which are defined here as extraordinary, strongly episodic floods in drylands generated by rainfall events of high volume and intensity. The occurrence of extreme floods during this period, which encompasses the Little Ice Age (LIA; CE 1400–1850), is coherent with other southern tropical datasets along the ITCZ over the last 2000 years, suggesting synchronous hydroclimatic changes across the region. This extreme flood period was preceded by several hundred years (P3: ~CE 700–1600) of less vigorous but more regular flows. The earliest period of the sediment record (P4: ~CE 100–700) was the most arid, with sedimentary and preservation processes driven by prolonged drought. Our results highlight the importance of developing paleoclimate records from the tropical and sub-tropical arid zone, providing a long-term baseline of hydrological conditions in areas with limited historical observations.

1. Introduction

There is increasing interest in using climate fluctuations over the last ~2000 years to place recent multi-decadal trends in the context of long-term change, including exploring the relative role of natural versus anthropogenic factors as drivers of change (e.g., Masson-Delmotte et al., 2013; PAGES 2K Consortium, 2013). However, determining the direction of change in the hydroclimate has been challenging in regions where there is a relative paucity of records and high spatial and interannual variability in rainfall. The situation is particularly acute in the Southern Hemisphere (Neukom and Gergis, 2012; Palmer et al., 2015). Paleo-studies and synthetic analyses have nevertheless identified significant and largely coherent shifts in tropical and sub-tropical hydroclimates during the late Holocene across Africa (e.g., Verschuren, 2004; Verschuren and Charman, 2008; Tierney et al., 2013), Central and South America (Haug et al., 2001; Hodell et al., 2005; Bird et al., 2011; Cuna et al., 2013), the Pacific (Sachs et al., 2009) and globally (Graham et al., 2011). Although sub-regional variations in tropical hydroclimatic trends have been recognised (e.g., Stager et al., 2013; Burrough and Thomas, 2013; Woodborne et al., 2015), there is a remarkable global coherence in hydrologic shifts for some periods, suggesting changes in the Intertropical Convergence Zone (ITCZ) (driven by Northern Hemisphere latitudinal temperature gradients) and/or the El Niño Southern Oscillation (ENSO) may play a role (Sachs et al., 2009; Graham et al., 2011; Schneider et al., 2014).

Strikingly, one of the most consistent features of synchronous changes in the tropics is associated with the cooler temperatures of the Little Ice Age (LIA) in the Northern Hemisphere (NH), defined here as a chronozone between CE 1400 and 1850 (PAGES 2k Consortium, 2013). A NH summer cooling is thought to have caused a southward shift or poleward expansion in the ITCZ and associated tropical rain belt (Broccoli et al., 2006; Yancheva et al., 2007; Sachs et al., 2009; Mohtadi et al., 2014). It has thus been hypothesised that the northern and southern tropics and sub-tropics experienced antiphase shifts in hydrology during the LIA: with drier (wetter) conditions in

77 the north mirrored by wetter (drier) conditions in the south (e.g., Haug et al., 2001; Verschuren,
78 2004; Sachs et al., 2009; Cuna et al., 2013).
79
80 Recent reviews of the Quaternary records from the Australian tropics and interior arid zone,
81 including marine sediments off the northwest coast that have been used to reconstruct relative
82 aridity and monsoonal dynamics during glacial and interglacial periods (van der Kaars and De
83 Deckker, 2002; van der Kaars, 2006; Stuut et al., 2011; De Deckker et al., 2014), surmising
84 increasingly arid conditions during the late Holocene (Fitzsimmons et al., 2013; Reeves et al.,
85 2013a, b). However, the resolution of these reconstructions is not sufficient to allow comparisons to
86 more recent hydroclimatic variation (e.g., Proske et al., 2014). A recent synthesis based on
87 Australasian records and modelling has proposed rainfall patterns over the Australasian tropics
88 followed a different trajectory to other continents during the late Holocene (Yan et al., 2015).
89 Unfortunately, the dearth of Australian terrestrial paleohydrological records with sufficient (sub-
90 centennial) temporal resolution is extremely limited, preventing the testing of hypothesised
91 asynchronous change in rainfall across the region and more broadly, the Southern Hemisphere
92 (Neukom and Gergis, 2012). In northwest Australia, for example, rainfall delivery today is
93 dominated by synoptic weather systems associated with the ITCZ, particularly tropical cyclones
94 (TCs) and monsoon lows (McBride and Keenan, 1982; Berry et al., 2011; Lavender and Abbs,
95 2013; Ng et al., 2015). The few published reconstructions, however, have had limited success in
96 extending the regional hydroclimate record. For example, speleothem $\delta^{18}O$ records from the
97 northwest coast spanning the last 1500 years have suggested the lowest level of cyclonic activity
98 over this period to be since 1960 in marked contrast to the weak observed relationship between
99 speleothem $\delta^{18}O$ and rainfall volume (Haig et al., 2014), observational trends (Shi et al., 2008;
100 Taschetto and England, 2009; Gallant and Karoly, 2010) and inferences over the last 150 years
101 from tree ring records from locations further inland (Cullen and Grierson, 2007; O'Donnell et al.,

2015). These contradictory findings clearly demonstrate the urgent need for further reconstructions from terrestrial environments across the region.

In this study, we report a new sedimentary record of climate variability for the past ~ 2000 years from the Fortescue Marsh, inland Pilbara (northwest Australia), a site known to capture regional hydroclimatic change resulting from flash surface flooding (Skrzypek et al., 2013; Rouillard et al., 2015). Our objectives were to (i) improve the temporal resolution and spatial coverage of late Holocene hydroclimatic variability in the northwest Australia and (ii) elucidate shifts involved in hemispheric circulation dynamics and associated patterns of rainfall that may relate to the LIA chronozone.

2. Methods

2.1. Regional settings and site description

The eastern Pilbara is located approximately 400 km inland of the northwest Australian coast (22°S 119°E; Fig. 1). The seasonal variability in rainfall is summer-dominated (Fig. 2), and interannual variability is one of the most extreme in the world (van Etten, 2009). The majority of rainfall is delivered over 1–5 days events by TCs and other closed lows. In contrast with South American and continental and west African Southern Hemisphere (SH) subtropics, the contribution of TCs to annual rainfall in the eastern Pilbara (30–40 %) is one of the highest globally (Dare et al., 2012; Lavender and Abbs, 2013; Ng et al., 2015). Evaporation rates in the catchment (~2800–3200 $mm \cdot yr^{-1}$) are up to ten-fold the average annual rainfall of ~290 mm (www.bom.gov.au/climate/data/).

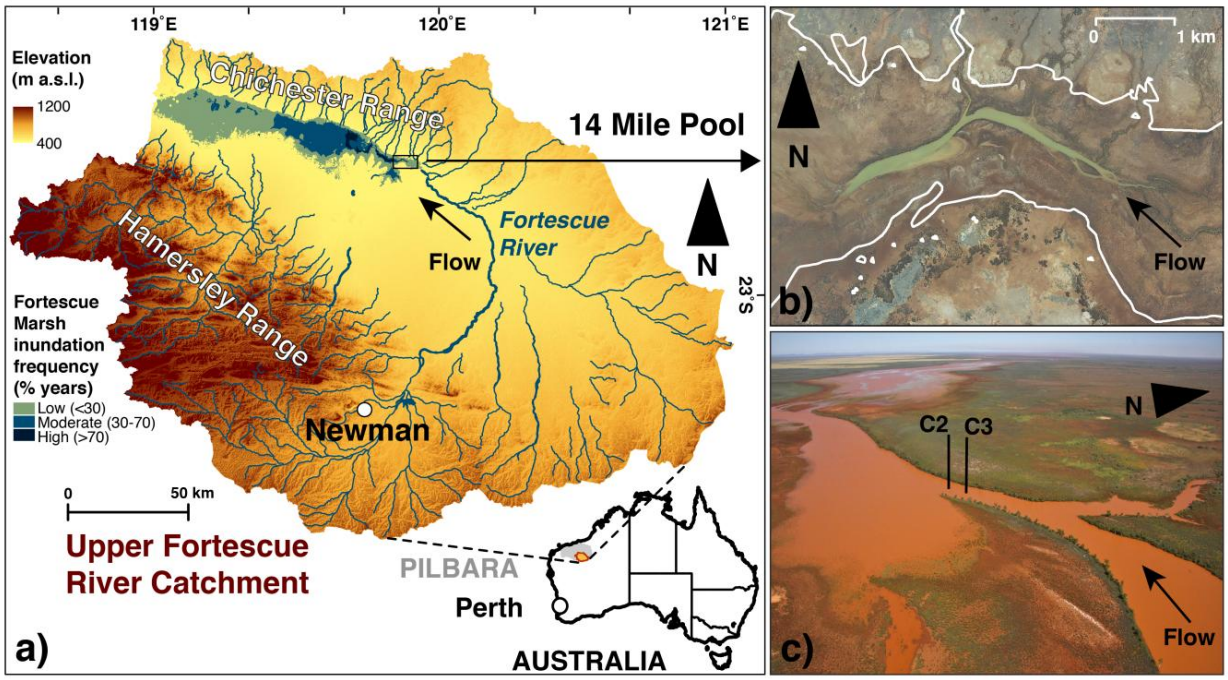

Figure 1: **a)** Topographic (1 Sec. SRTM Derived DEM-H v.1; Geoscience Australia) and (intermittent) river network (Geoscience Australia) map of the Fortescue Marsh catchment (i.e., Upper Fortescue River catchment), including the present study site (14 Mile Pool), and frequency of inundation of the Marsh (modified from Rouillard et al., 2015); **b)** 40 cm resolution ortho-photo (July 2010; Fortescue Metals Group Ltd) overlaid by maximum 1988–2014 floodplain (solid white line; Rouillard et al., 2015); **c)** aerial photograph taken on Feb 2012 (A. Rouillard) showing the coring location of replicate cores FOR106C2 (C3) and FOR106C3 (C3).

(2-COLUMN FITTING IMAGE)

The Fortescue Marsh (hereafter referred to as the Marsh and known as *Martuyitha* to indigenous peoples) lies in the Fortescue Paleovalley, which is flanked by the Chichester and Hamersley ranges. The Marsh acts as a terminal basin for the Upper Fortescue River catchment (30,000 km^2; Fig. 1a). The Upper Fortescue River catchment, including the Marsh, is not hydrologically connected to the Lower Fortescue River catchment (Skrzypek et al., 2013). The Fortescue River drains 56 % of the Upper Fortescue River catchment where it reaches the Marsh (Fig. 1a). Gauging stations in the catchment are limited; however, a continental-scale classification of stream and river flow regime based on <20 years of discharge records in the region described flow as being 'variable summer extremely intermittent' (Kennard et al., 2010). This flow regime class is the most extreme

144 on the Australian continent and is described by the highest number of zero flow days (>250 per
145 year), lowest baseflow index, highest variability and skewness of daily flows, and in the timing of
146 maximum flows, highest rise and fall rate (up to ~20 and 5 ML day^{-1} day^{-1}, respectively). This
147 extreme regime also has predictable high flows (>1st percentile) with daily volumes in excess of
148 15 ML day^{-1}.
149
150 We extracted sediment cores from 14 Mile Pool, a relatively large pool located on the eastern
151 boundary of the Fortescue Marsh (Fig. 1). The generally shallow (< 2 m) pool represents a terminal
152 reach (~2 km long) of the Upper Fortescue River at the head of the Marsh (Fig. 1a), 14 Mile Pool is
153 the most frequently inundated and perennial water feature of the Marsh and receives most of the
154 flow that subsequently progresses west across the floodplain (Rouillard et al., 2015). The hydraulic
155 gradient along the Upper Fortescue River between Newman and 14 Mile Pool is 0.0007. To the
156 north, 14 Mile Pool drains a section of the Chichester Ranges (hydraulic gradient of 0.006, and
157 0.003 over the immediate 15 km), which represents only 3% of the pool's total catchment area. 14
158 Mile Pool was selected after an extensive coring survey across the Marsh and along the major creek
159 lines upstream in the Upper Fortescue River system; at other sites surveyed, sediment sequences
160 were either mixed vertically (fine particles, silty clays in claypans on the floodplain) or clearly
161 scoured by high energy flash floods (i.e., coarser particles, sandy and gravelly beds of pools higher
162 up in the ranges).
163
164 The bed of the pool at the coring location is ~75 m wide (~405.5–406 m a.s.l.) and overflows on to
165 a 1400 m wide floodplain (407–407.5 m a.s.l.) during short-lived flooding events (Fig. 1b). The
166 inundation regime at the Marsh over the last 100 years has been strongly dominated by TC-
167 generated, high-volume summer rainfall events resulting in flash floods (Rouillard et al., 2015).
168 Between 1988 and 2012, surface water on the 14 Mile Pool and floodplain typically receded to the
169 pool's bed and became isolated from the Upper Fortescue River within a month of flooding, but on
170 average remained connected to the other downstream sections of the Marsh for 3–4 months every

171 year. During large wet years (>300 km^2 inundations), which occurred about once in 10 years over
172 the last century, downstream connectivity of 14 Mile Pool with the Marsh persisted for up to 10
173 months (Rouillard et al., 2015).
174
175 Water chemistry measurements taken between 2010 and 2012, including quantification of
176 evaporative loss using water stable isotopes and ionic concentration of salts, show that 14 Mile Pool
177 experiences large shifts in volume (i.e., depth, width and length) in response to flooding and
178 seasonal or prolonged supraseasonal drying rather than being sustained by groundwater (Skrzypek
179 et al., 2013). Fresh, slightly acidic, softwater and nutrient poor conditions brought by flooding
180 progressively develop into brackish (total dissolved solids = 60–6000 $mg \cdot L^{-1}$), alkaline (pH=6.6–
181 9.9), hardwater (HCO_3^-=23–308 $mg \cdot L^{-1}$) and slightly enriched in nutrients (total filterable
182 phosphorus = <0.01–0.2 $mg \cdot L^{-1}$; total filterable nitrogen = 0.4–4 $mg \cdot L^{-1}$) over time as water
183 evaporates. Daytime water temperature varies between 13–36˚C. Turbidity of the pool is at its
184 highest within the month following flooding (10–240 NTU), and during the dry winter season when
185 the pool is most shallow. However, the water column clears very quickly once flooding subsides as
186 clays settle to the bottom of the pool enabling algal and macrophytic growth.
187
188 14 Mile Pool is flanked by a narrow band of riparian vegetation on both banks dominated by large
189 *Eucalyptus camaldulensis* and *E. victrix* trees (Fig. 1c). Beyond the riparian corridor, salt-, drought-
190 and inundation-tolerant succulents (*Tecticornia* and other chenopods) dominate the floodplain
191 vegetation (Beard, 1975). Early cadastral maps (Fig. A.1; Dept of Lands and Surveys, 1892, 1894,
192 1899, 1905a,b, 1909, 1919, 1921, 1924, 1952), aerial photographs (1957; Edward de Courcy Clarke
193 Earth Science Museum, UWA) and high-resolution ortho-rectified imagery (2004, 2006, 2010,
194 2012 and 2013; www.landgate.wa.gov.au) indicate that there has been no major change in the site
195 location (1892) and morphology (1905) of 14 Mile Pool since at least this period (i.e., coverage of

196 the earliest cadastral map available for the area showing the position of a watering point at current
197 location; Fig. A.1).
198

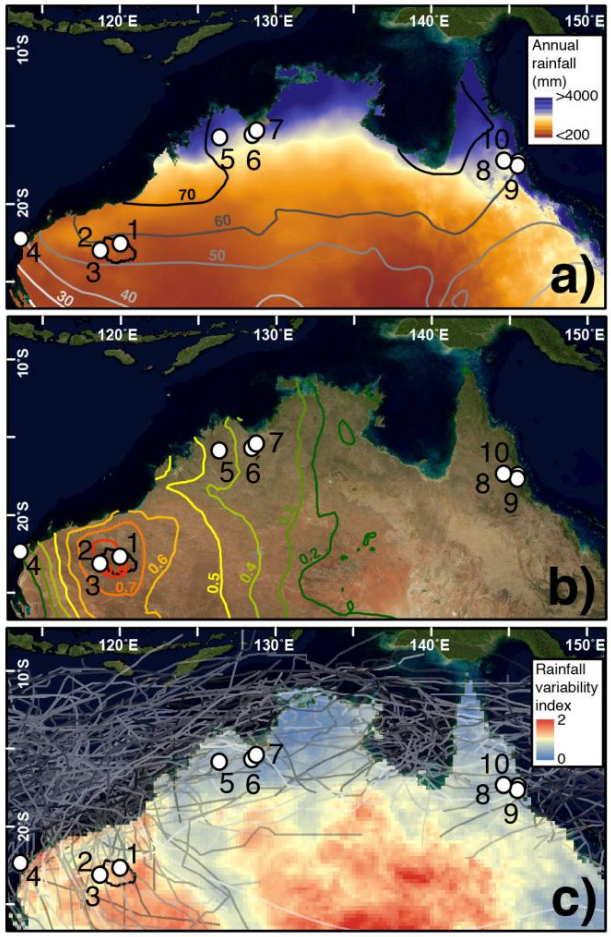

199
200 **Figure 2**: **a)** annual rainfall (shading), proportion (%) of average annual rainfall that falls in Jan–
201 Mar (isohyets; www.bom.gov.au) and locations of published terrestrial paleohydrological records in
202 tropical and subtropical Australia with sub-centennial resolution discussed in the text, including (1)
203 Fortescue Marsh, present study; (2) Juna Downs (Cullen and Grierson, 2007); (3) Hamersley Range
204 (O'Donnell et al., 2015); (4) Cape Range and (8) Chillagoe (Haig et al., 2014); (5) Black Springs
205 (McGowan et al., 2012); (6) KNI-51 (Denniston et al., 2013; 2015); (7) King River (Proske et al.,
206 2014); (9) Bromfield Swamp and (10) Mount Quincan (Burrows et al., 2014); overlaid on Upper
207 Fortescue River catchment (black line); **b)** April true colour MODIS composite image (Blue Marble
208 Next Generation with Topography; www.visibleearth.nasa.gov/view.php?id=74318) and isohyets of
209 the correlation strength (R^2) between summer rainfall and Hamersley Range tree rings growth
210 (modified from O'Donnell et al., 2015), and **c)** interannual variability in rainfall (www.bom.gov.au)
211 and 1979–2012 TCs tracks (Tropical Cyclones Database; www.bom.gov.au/cyclone).
212 **(1-COLUMN FITTING IMAGE)**

213

214 ***2.2. Core collection and processing***

215 Two 0.6 m replicate sediment cores (codes FOR106C2 & FOR106C3; 22˚33'20.4"S 119˚51'40.9"E
216 & 22˚33'19.2"S 119˚51'42.3"E, respectively) were extracted 50 m apart below 1.8 m of water
217 (bank full) in November 2011 from the deepest section of 14 Mile Pool (Fig. 1c) using a modified
218 percussion corer activated from a floating platform. To select the coring location, we surveyed
219 satellite imagery over the 1988-2012 period (Rouillard et al., 2015) to observe seasonal drying
220 sequences of the 14 Mile Pool and to determine the most frequently and most persistent inundated
221 section of the pool. Briefly, all the captured imagery from the *Landsat* archive over our study site
222 was compiled and analysed, with episodic coverage between 1972-1988 and nearly fortnightly
223 resolution between 1988-2012 (see Rouillard et al. 2015 for further details). We also conducted
224 seasonal field surveys over the 2009-2012 period, including quantification of evaporative loss using
225 water stable isotopes and ionic concentration of salts, which confirmed large variation in water
226 volume of the pool (i.e., depth, width and length) in response to flooding and seasonal or prolonged
227 supraseasonal drying and that only the location chosen for coring remained inundated. Bathymetric
228 assessment confirmed that cores were obtained from the deepest section of the 14 Mile Pool
229 (Sep. 2011). We also conducted a second coring survey in November 2012 in the same section of
230 the pool (at the location of FOR106C3), where two percussion cores (to compacted base layer; ~60
231 cm) and two hand pushed cores (~20 cm) were taken from the floating platform in only 50 cm
232 water depth. These cores confirmed a coherent longitudinal lithology in the section that was
233 consistent after a major flood event. In summer 2012, TC Heidi (Jan 11–13) generated up to
234 184 mm of rain overnight in the Upper Fortescue catchment that we estimated, based on data
235 collected from newly installed piezometers across the Marsh, resulted in >400 GL of water to the
236 Marsh. However, the sequences extracted before (Nov 2011) and after this large flood (Nov 2012)
237 had the same apparent lithology, including distinct, sub-cm horizontal layering in the top 5 cm of
238 the core.

239

240 Despite multiple coring attempts, longer sediment profiles could not be retrieved due to an
241 underlying cemented layer. The 5-cm diameter cores were split lengthwise in the lab using a
242 rotating saw and stainless steel wire and the texture, layering and colour of the split cores were
243 characterised visually. One half was wrapped in plastic and aluminium foil and preserved at 4˚C as
244 a reference. The other half was sub-sectioned in 1 cm thin slices. Subsamples from the centre
245 portion (diameter ~ 3 cm) that had not been in direct contact with the PVC piping were placed in
246 aluminium foil and used for dating and isotope analyses, while the outer portion of the 1 cm
247 sections were bagged and used for microfossil and granulometric analyses. All discrete intervals
248 were frozen at −20˚C directly prior to freeze-drying for measurement of moisture content.
249 Mineralogy was established using X-ray diffraction (XRD) on random powder using a Philips
250 PW3020 diffractometer at depths 8, 46 and 57 cm (FOR106C3).
251

252 *2.2.1. Particle size analysis*

253 Particle characterisation was made on FOR106C3 using a series of phi stainless steel sieves. Prior
254 to sieving through a 1 mm mesh sieve, the sediment was screened for macrofossils and the > 1 mm
255 fraction analysed for particle size. An aliquot (~0.5 cm^3) of the <1 mm fraction was analysed in
256 Calgon ($Na_6O_{18}P_6$) using a Malvern Mastersizer 2000 with Hydro2000G light scattering laser
257 counter. Measurements were made in triplicate and average values were used to build a frequency
258 histogram. GRADISTAT v.4.0 software (Blott and Pye, 2001) was used to calculate the statistical
259 grain size parameters (mean, median, sorting/standard deviation, sand, silt, clay and gravel
260 percentages) on the integrated >1 mm and <1 mm fractions using the method of moments with
261 geometric scaling.
262

263

264 *2.2.2. Total C and N and stable isotopic signatures*

265 Total C and N (%) contents and stable isotope signatures (δ^{13}C and δ^{15}N) of the <1 mm fraction of
266 every 1-cm interval (FOR106C3) were obtained using a Thermo Flush Elemental Analyser coupled
267 with a Delta V Plus Isotope Ratio Mass Spectrometer (Thermo Fisher Scientific, Bremen,
268 Germany) at the West Australian Biogeochemistry Centre at The University of Western Australia
269 (www.wabc.uwa.edu.au). All samples were freeze-dried, ground and homogenized prior to analyses.
270 Sediment organic carbon (OC) content and δ^{13}C were also determined for every other interval of the
271 60-cm long profile (FOR106C3). Following standard protocols, app. 100-150 mg was pre-treated at
272 room temperature overnight with acid (4 % HCl) to remove carbonates (Brodie et al., 2011).
273 However, acid pre-treatment for the removal of inorganic carbon (IC) commonly introduces biases
274 in δ^{13}C and C estimates beyond instrumental precision (e.g., 4 ‰; Brodie et al., 2011). Given the
275 very low total C content of our samples and the low variability they showed in δ^{13}C (generally
276 <1 ‰), the removal of IC for determination of bulk OC content and δ^{13}C values was considered
277 unreliable. Thus, we report our findings as non-acidified. All stable isotope analyses have been
278 reported in permil (‰) after multi-point normalization to international scales using NBS19,
279 USGS24, NBS22, LSVEC for δ^{13}C and IAEA-N1, IAEA-N2, USGS32 for δ^{15}N (Skrzypek, 2013),
280 with combined analytical uncertainty of <0.10 ‰. Correction of total content of C and N was
281 applied to account for the proportion of the weight of the <1 mm fraction.
282
283 *2.2.3. Subfossil analysis*

284 Where present, ostracod shells were systematically sampled from the full core for every 1-cm
285 interval of the loose freeze-dried sediment for identification (FOR106C3). The extensive iron oxide
286 coating was individually removed from the shells in a sonication bath of deionised water (10
287 seconds). After a coarse resolution (10-cm) analysis for microfossils, pollen of *Chenopodicaeae,*
288 *Poaceae, Myrtaceae* and *Asteraceae* families were identified. Overall pollen concentrations were
289 found to be very low (averaging ~5000 grains·cm^{-3}; Shulmeister, 1992), however, and no pollen

290 was found in the basal samples. Preservation rates were also very low, with <20% non-deteriorated
291 grains per interval in the majority of cases. Deteriorated grains were primarily crumpled, most
292 likely reflecting mechanical damage resulting from compaction, inwash or sediment disturbance
293 through, for example, rewetting and subsequent drying of the sediment cracking clays (Cushing,
294 1967; Lowe, 1982), which also corresponded with the results of preliminary diatom analysis. Given
295 the low concentrations coupled with high levels of deterioration evident in the sequence, it was
296 determined likely that the non-deteriorated microfossils would represent types more resistant to
297 decay, rather than past assemblages per se.
298
299 ***2.3. Developing a chronological framework***
300 A geochronological framework for the sequence was established using ^{210}Pb, ^{137}Cs and accelerator
301 mass spectrometry (AMS) ^{14}C radioisotopic techniques (Appleby, 2001; Björck and Wohlfarth,
302 2001). ^{210}Pb and ^{137}Cs activities were measured on ~2 cm^3 freeze-dried sediment from 18 intervals
303 of replicate core FOR106C3 using gamma counters at the Paleoecological Environmental
304 Assessment and Research Laboratory (PEARL, Queen's University, Kingston, Ontario, Canada)
305 following Schelske et al., (1994). AMS ^{14}C dating was performed at the STAR facility at the
306 Australian Nuclear Science and Technology Organisation (ANSTO) at Lucas Heights, NSW
307 Australia (Hua et al., 2001; Fink et al., 2004) and Waikato Radiocarbon Dating Laboratory
308 (Hamilton, New Zealand). Given the consistent lithologies between replicate cores FOR106C2 &
309 FOR106C3, eight terrestrial plant macrofossils (fresh and charred) and six bulk samples were
310 extracted from both cores for AMS ^{14}C analysis: depths from FOR106C2 were converted to
311 FOR106C3 depths by linear interpolation between distinct lithological sections. Radiocarbon ages
312 were calibrated to Common Era (CE) years using atmospheric bomb ^{14}C data for the Southern
313 Hemisphere (SH) Zone 1-2 (Hua et al., 2013) and extended back in time by the SHCal13 calibration
314 curve (Hogg et al., 2013) and OxCal v. 4.2 program (Bronk Ramsey, 2009). Unless explicitly
315 described otherwise, ages mentioned henceforth are quoted in CE years.

316 **3. Results**

317 ***3.1. Age-depth models***

318 The three dating techniques employed (^{210}Pb, ^{137}Cs and ^{14}C) provided coherent chronologies for the
319 sequence. As might be expected for such arid and extreme hydrologic conditions, sedimentation
320 rates were not linear and the sequence is likely discontinuous (Figs. 3; 4). ^{210}Pb and ^{137}Cs activity
321 concentrations, used for the most recent history of the sequence, were both low (values below 100
322 and 5 Bq·kg^{-1}, respectively) but comparable to other lacustrine sediments from the SH (Gell et al.,
323 2005; Leslie and Hancock, 2008). Total ^{210}Pb activity for the 13 samples analysed generally
324 declined with depth but several inversions from this trend were also evident (Fig. 4a). Below 40 cm
325 depth the unsupported ^{210}Pb activities were too low to be used in the dating calculations, whereby
326 total ^{210}Pb activities were not significantly different from supported ^{210}Pb activities, estimated (i.e.,
327 averaged) to be ~30 Bq·kg^{-1}. In the top 40 cm of the core, the lower unsupported ^{210}Pb activities
328 ('low activities' sample series; Fig. 4a), were not used either as these activities may represent older
329 sediment materials from the catchment being re-deposited over more recent materials during large
330 floods ('dilution effect'; Appleby, 2001) or some level of re-suspension and mixing at the sediment-
331 water interface. This interpretation of the irregular depositional pattern is supported by the
332 lithological layering, where we observed an abrupt horizontal colour and grain size change in this
333 section of the core (Fig. 3). Additional variability in the supported ^{210}Pb activities (background) can
334 also be seen from the uneven ^{214}Bi profile (Fig. 4a). Thus, only the five top samples (8 to 33 cm)
335 with higher unsupported activites ('high activities' sample series; Fig. 4a, b) representing 'non-
336 flood related depositions' were used in the chronology reconstruction.
337
338
339

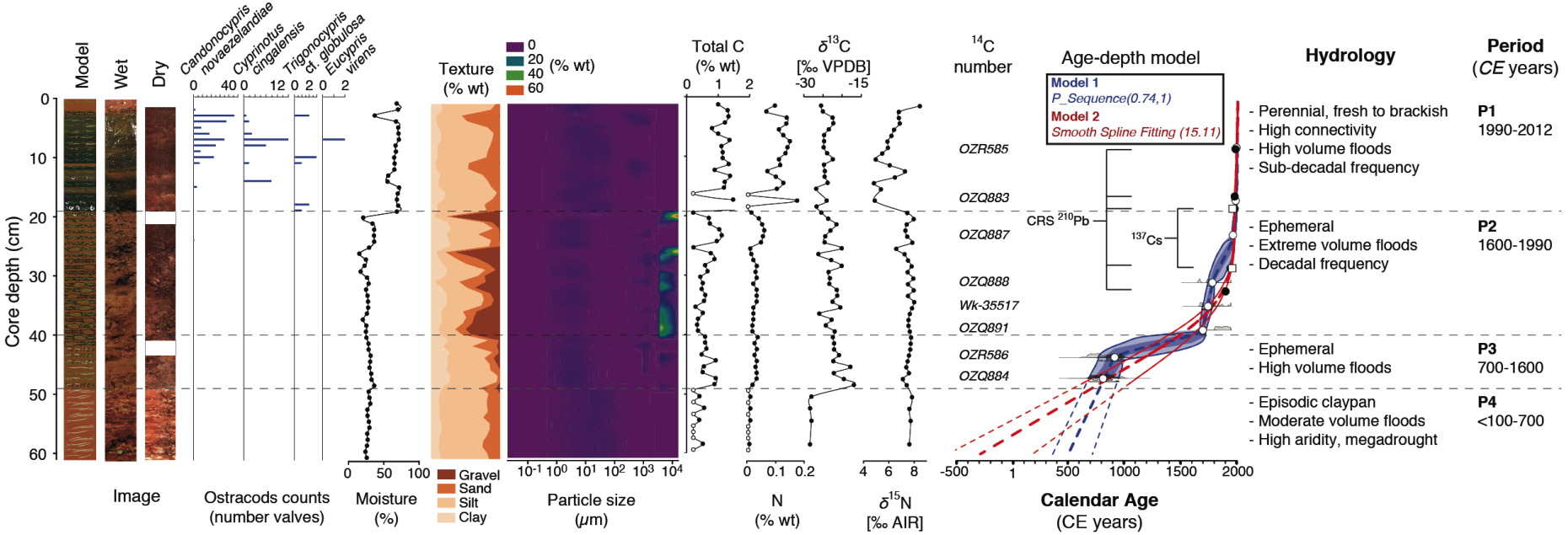

Figure 3: Stratigraphy of 14 Mile Pool core. From left to right: schematic representation (Model); high-resolution photographs (Wet and Dry); number of ostracod valves; moisture content (% weight); statistical grain-size parameters (gravel, sand, silt and clay fractions; % volume < 1 mm; % weight > 1 mm) (GRADISTAT 4.0; Blott and Pye, 2001); grain size 3D surface plots (z axis = % volume < 1 mm; % weight > 1 mm); total C and N content (% weight); bulk $\delta^{13}C$ [‰ VPDB] and $\delta^{15}N$ [‰ AIR], laboratory codes for AMS ^{14}C age estimates (^{14}C number); age-depth Bayesian P_Sequence Model 1 rived from ^{14}C ages only (blue series; OxCal v. 4.2; Bronk Ramsey, 2009) and Smooth Spline Fitting Model 2 based on all ages including ^{210}Pb, ^{137}Cs and ^{14}C (red series; CLAM; Blaauw, 2010), with respective 95% confidence intervals envelopes and model extrapolations (<48 cm depth), ^{14}C age estimates (open circles) and their probability distributions (2σ envelope in grey; OxCal v. 4.2), Constant Rate of Supply (CRS) ^{210}Pb (closed circles) and ^{137}Cs (squares) age estimates; hydrological interpretation; and time period (transitions estimated from the average values provided by Models 1 & 2 in the adjoining intervals).

(FULL HORIZONTAL FITTING IMAGE)

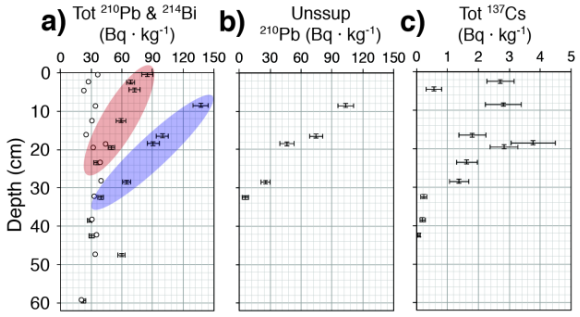

Figure 4: Gamma counting results from 14 Mile core (FOR106C3), including **a)** total ^{210}Pb (with error bars) of all analysed intervals, including the selected 'high activities' (blue shading) and discarded 'low activities' (red shading) sample series for the age calculations and ^{214}Bi activity (i.e., a proxy for supported ^{210}Pb; open circles); **b)** unsupported ^{210}Pb activity (with error bars) included in age-depth Model 2 (see Sect. 3.1 for details of selection); and **c)** total ^{137}Cs (with error bars).

(1-COLUMN FITTING IMAGE)

Based on these five selected samples, the Constant Initial Concentration (CIC) and Constant Rate of Supply (CRS) models provided close agreement on ^{210}Pb age determinations (i.e., within analytical uncertainties); the CRS was ultimately selected as it was better suited to the variable accumulation rate of this core (Appleby, 2001). For verification of sample selection in the top 40 cm of the core, we also calculated age estimates from the discarded 'low activities' samples as an independent series but found no difference in estimates between series (Fig. 4a). The highest ^{137}Cs activities were measured between 16.5 and 19.5 cm, delineating a depth range for the peak nuclear testing of 1964 in the SH (Fig. 4c) and supporting the calculated CRS model ^{210}Pb chronology (Leslie and Hancock, 2008). The onset of ^{137}Cs was identified at 28–29 cm, which should correspond to the early detection of ^{137}Cs fallout from nuclear testing (CE 1954–1957) (Leslie and Hancock, 2008).

373 Two age-depth models were constructed for the sequence (Fig. 3). The surface was
374 assigned as CE 2012 as the date of coring as it immediately followed a major flood
375 event (Rouillard et al., 2015). The first age-depth model (Model 1) was based on the
376 eight radiocarbon dates of terrestrial macrofossils (Fig. 3; Table A.1; A.2). Bulk
377 samples yielded older ^{14}C ages compared to those of terrestrial macrofossils at the
378 same depths, possibly reflecting a hard water effect as a result of carbonate bedrock
379 (Björk and Wohlfarth, 2001) and/or transportation of older (reworked) material from
380 the catchment. However, the offset that could be attributed to the reservoir effect was
381 not constant through time, ranging from 240 to 2483 yr (Table A.1). Considering the
382 high level of biological reworking of organic material that takes place in arid
383 environments, it is likely that the bulk-dated organic compounds were highly
384 recalcitrant terrestrial compounds transported from the surrounding catchment during
385 flooding and/or preferentially preserved with depth mixed with a variable amount of
386 organic matter (OM) produced in situ (Battin et al., 2008). Thus, bulk samples were
387 not used for the age-depth models (Table A.1, A.2).
388
389 We used two approaches to estimate the age of the sediments from 14 Mile Pool.
390 Model 1 was built using the Bayesian P_Sequence model in the OxCal program v. 4.2
391 (Bronk Ramsey, 2009) with a low *k* value of 0.7 to allow flexibility in the model
392 (Fig. 3). The overall agreement index of the model was 59 %, which is very close to
393 the accepted level of 60 % (Bronk Ramsey, 2008). The second age-depth model
394 (Model 2), which includes ^{14}C (8), CRS ^{210}Pb (5) and ^{137}Cs (2) age estimates, was
395 performed in CLAM (Blaauw, 2010) using smooth spline fitting with a goodness-of-
396 fit of 15.11 (Fig. 3). The main differences in the outputs of the models are in the age
397 estimation of the P3–P2 boundary and the early onset of the profile; Model 1 places

these boundaries at ~150 and 800 years later than Model 2, respectively. Given the sequential but likely discontinuous depositional patterns of the system (intermittent sedimentation and transport) and the effect of sub-aerial drying on the sequence (weathering, wind deflation), these age-depth models have been applied here to provide age estimates of the boundaries for key hydrologic periods (described here as P1–4) and sedimentation rates (averaging between models). More detailed implications of sequence discontinuities and the differential between models on boundary estimates for paleohydrological interpretations are discussed below for each period.

3.2. Multi-proxy paleohydrological reconstruction

All age-depth models identified several inflections in sedimentation (Fig. 3). Four stratigraphic units (P1–4) were identified from shifts in sediment accumulation rates and other sediment properties (i.e., particle size distribution, moisture content, oxidation state, macrofossil abundance and C and N content and stable isotopes) (Fig. 3), which most probably indicate different hydrological conditions in the four periods. These different hydrological regimes may either reflect the catchment hydroclimatic history, shifts in catchment processes affecting runoff and erosional patterns from land use (post 1860s) or a morphological shift in the river channel position through lateral displacement or an avulsion event (Jones and Schumm, 1999). Avulsion events (when the old river channel is abandoned and a new river channel is formed) are well documented elsewhere on low gradient floodplains in the arid zone (e.g., Ralph et al., 2011; Donselaar et al., 2013). However, they are unlikely at 14 Mile Pool given the local geomorphological conditions described above (topography, soil type, stability of long-lived vegetation on banks) and the consistency in the observed mineralogical profile (Figs. 1, 4). The mineralogy of the sequence was

dominated by alumina-silicate clays ('cracking clays') with a smaller proportion of iron oxides and consistent with depth (i.e., the mineralogy was almost always mainly kaolinite and quartz with moderate amounts of illite (hydromuscovite), goethite, and hematite). The strong relationship between rainfall variables and surface water hydrology at the Marsh over at least the last 30 years also suggests these processes would have a relatively low influence on runoff in comparison to the hydroclimate (Rouillard et al., 2015).

3.2.1. Stratigraphic changes over the last 2000 years

3.2.1.1. Period 1 (P1)—CE 1990 to present: A perennial water hole in the desert

The uppermost sediments (<19 cm) clearly capture a relatively fast (i.e., the highest in the record), sequential but irregular aggradation of alluvial sediment (0.3–0.6 $g \cdot cm^{-2} \cdot yr^{-1}$) in a perennial, aquatic environment, encompassing the last ~20 years (average age of 18-20 cm transition from models 1 and 2 = 1991). The dilution pattern identified from the ^{210}Pb chronology (Appleby, 2001) suggests high-energy flooding of the pool contributed transported sediment from the upstream floodplain to the sequence (Fig. 4). The anoxic muds (inferred from the oxidation of the sediment once in contact with air), relatively high moisture content (>50 %), abundance of well-preserved ostracods and presence of plant and other macrofossils combined with smaller grain size (<1 mm) and relatively high nitrogen content (mean = 0.12 % dry wt; range = 0.06–0.17 %) all suggest that 14 Mile Pool received regular inflows of water of small to high energy during this period (Fig. 3). A sedimentary water content of ~70 %, however, is rather low for recent subaqueous lacustrine deposits but not unexpected considering the very low organic content (Verschuren, 1999; Bessems et al., 2008).

449

450 The slight depletion on average in both $\delta^{15}N$ (−1.4 ‰) and $\delta^{13}C$ (−1.3 ‰) in this
451 period compared to the remainder of the profile further indicates a change in
452 biogeochemical processes in this period. The low total C content detected in the
453 Fortescue Marsh sediments (<1 %) was similar to modern Pilbara soils and typical of
454 sediment of dry stream beds (Ford et al., 2007; McIntyre et al., 2009a, b; Siebers et al.
455 2015). Lower $\delta^{13}C$ values of the bulk sediment (−24.4 ‰) compared to the remainder
456 of the core (−23.0 ‰) as well as higher C content for this record (mean = 1.4 %;
457 range = 0.8–5.6 % wt; Fig. 3) suggest a relatively higher organic input (or lesser
458 inorganic input, i.e., carbonates) compared to the typically more enriched carbonates
459 (Finlay and Kendall, 2008). Alternatively, this change may reflect a lower input of
460 OM with more positive $\delta^{13}C$ signatures such as C_4 grasses (−6 to −23 ‰) as opposed
461 to C_3 plants (−23 to −34 ‰) (Schidlowski 1987). Higher organic content in the
462 sediment is consistent with relatively wetter conditions, where autochthonous primary
463 production increases as a result of more frequent prolonged clear and fresh water
464 phases (Coianiz et al., 2015). Wetter conditions may also result in: (i) increased
465 production and transport of terrestrial OM from the catchment to the site through
466 increased runoff (Battin et al., 2008); (ii) better preservation of OM under persistent
467 anoxic conditions and limited sub-aerial oxidation of the clay-rich sediment
468 (Verschuren, 1999); or (iii) a combination of these mechanisms. Bulk $\delta^{15}N$ data
469 should always be interpreted along with other evidence as sediment sequences are
470 complex and may be influenced by diagenesis and anthropogenic depositions
471 (Brahney et al., 2014). Consequently, the lower $\delta^{15}N$ values in this context may
472 reflect (i) the fixation of atmospheric N_2 by cyanobacteria or (ii) diagenetic microbial

processing of in the sediment that would be favoured under perennial conditions (Brenner et al., 1999; Gälman et al., 2009).

Ostracods were only recovered from the top 19 cm of the core (with single valve found at 24 cm), corresponding to the period of ~1990 to 2012 (P1, Fig. 3). This high level of preservation in P1 also suggests limited drying during this period. Though the clay-rich sediment form a relatively impermeable streambed, prolonged drying would have caused any valves that may have been deposited previously to be gradually dissolved by slightly acidic rainwater occasionally percolating through the dry sediment. The two dominant ostracod species identified (*Candonocypris novaezelandiae,* Baird, 1843; *Cyprinotus kimberleyensis*, Karanovic, 2008) in the top 15 cm of this period (Fig. 3) are freshwater species. The presence of male specimens of *C. novaezelandiae* in particular indicate more permanently inundated conditions because male offspring are only produced in favourable conditions (Radke et al., 2003). The presence of the resting stages of Cladocerans (i.e., epphippia) also suggests limited seasonal drying as these are micro-crustaceans that are generally absent in systems where droughts longer than 6–20 years occur (Jenkins and Boulton, 2003). This finding suggests that either annual summer inundations were large enough to maintain the aquatic habitat until the next rain season through significant recharge of the shallow river alluvium, or smaller pulses throughout the year contributed to the persistence of the surface water. The inundation extent at the Marsh over the last century (Rouillard et al., 2015) suggests a combination of both of these recharge patterns contributed to maintain the aquatic habitat. The coherent age-depth profile of P1 (Fig. 3) further indicates that any of the extreme flood events over the last ~20 years (Rouillard et al., 2015) were of insufficient energy to scour the

498 sediment down to the bed of the pool. The onset of P1, however, may have been
499 abrupt, as indicated by the presence of several land snail shells at the transition (18–
500 20 cm) that were also found along the flood margins of the Marsh floodplain
501 following the large inundation related to TC Heidi (Jan 2012).
502
503 *3.2.1.2. Period 2 (P2)—CE 1600–1990: Extreme floods*
504 Period 2 (CE ~1600–1990; 19–40 cm; Fig. 3) is most remarkable due to an abrupt and
505 major change in sedimentology that reflects a much higher energy environment and
506 likely more variable hydrology than P1, P3 or P4. This period (P2) is characterised by
507 a heterogeneous particle size matrix as well as the coarsest material in this record, i.e.,
508 fine to coarse (up to 2 cm) pebbles (Fig. 3). Virtually no microfauna were preserved
509 in the sediments of this period. Total C (mean = 0.6 % wt; range = 0.2–1.1 % wt) and
510 N (mean = 0.03 % wt; range = 0.01–0.06 % wt), while less than in P1, were also
511 higher than either P3 or P4. Extreme flooding (i.e., much higher energy than P1)
512 would have been necessary to carry the coarser bed load materials during this period,
513 especially since the site is on a low gradient that should cause the erosion threshold to
514 be relatively high (Powell, 2009). Coeval ^{14}C age determinations for the oldest part of
515 this period (Table A.1) as well as the lower sedimentation rate for P2 (0.07–0.1 $g \cdot cm^{-2} \cdot yr^{-1}$)
516 compared to P1 further suggest that extreme flooding might have occurred
517 within a narrow time window as opposed to over the entire period, each event causing
518 some degree of scour-induced hiatus(es) and mixing of the sediment (Fig. 3).
519 Scouring of the sequence, specifically of the most recent portion of P3, could also
520 explain the apparent abrupt in sedimentation rate between P2 and P3 (Fig. 3).
521 Sedimentary water content as low as 30-40 % (Fig. 3) can only be explained by one or
522 more episodes of prolonged drying (i.e., greater than current period) during the

523 deposition of units P4-P2. Sub-aerial oxidation during those dry episodes explains, at
524 least in part, the extremely low total C and N (Fig. 3; Verschuren, 1999), although
525 both C and N contents in soils of the surrounding catchments are also invariably very
526 low (Ford et al., 2007).
527
528 Given the low hydraulic gradient (i.e., 0.0007 over 100 km along the Upper Fortescue
529 River to the east and, of lesser significance, 0.006 over 30 km to the north) of the
530 pool's upstream floodplain and because relatively higher volume and/or more intense
531 events would have been necessary to generate the shift in sedimentary patterns (i.e.,
532 pebble-sized particles, scouring) observed in P2 compared to the other periods of this
533 record including documented very intense and high volume floods in the last 100
534 years, we describe these flooding events as 'extreme floods'. System memory or
535 water storage has also been shown to significantly influence runoff and wetland
536 inundations at the interannual level in arid environments worldwide (Reaney, 2008;
537 Shook and Pomeroy, 2011). Here, the high energy floods during P2 would be
538 consistent with more severe and/or intense rainfall events that likely followed
539 prolonged periods of drought and resulted in supraseasonal-inundated conditions on
540 the Marsh (Rouillard et al., 2015). In arid landscapes where soils are dominated by
541 relatively impermeable clays, drought conditions cause vegetation cover to become
542 sparser and can increase overland flow and flash runoff response (Sutfin et al., 2014).
543 This interpretation would explain why the more perennial conditions of the pool
544 during this period did not enable major scouring to occur, despite the multiple
545 documented severe inundation events post-1990 at the Marsh (Rouillard et al., 2015).
546 Owing to the large size of the material transported and deposited in to the 14 Mile
547 Pool, we hypothesise that the size of these flood events in P2 were also likely larger

548 than any observed over at least the last two decades (Rouillard et al., 2015; Fig. 3).
549 We suggest the more intense floods captured by our multiproxy analysis in P2
550 compared to the remainder of the profile were caused by one or more episodic heavier
551 and short-lived rainfall events, within an overall background of drier conditions.
552
553 The Pilbara has undergone relatively little change in catchment land use until the
554 advent of mining in the region in the 1960s. Nevertheless, localised cattle and sheep
555 grazing and the introduction of invasive grass species, as well as shifts in burning
556 practices, might have influenced sedimentation rates of the 14 Mile Pool over the past
557 century, as has been extensively documented elsewhere in the arid zone (e.g., Adair
558 and Burke, 2010; Dunne et al., 2011; Eldridge et al., 2012). For example, pastoral use
559 of 14 Mile Pool as a water point for sheep and cattle started in the late 1870s (Western
560 Mail, 1917), and a stocking route went along the Fortescue River on the floodplain
561 ~20 km upstream of the Pool (Fig. A.1). Stocking numbers peaked around the 1930s
562 in the area (www.trove.nla.gov.au; McKenzie et al., 2009). Increased erosion along
563 floodways was also reported in the Pilbara along with changes in vegetation in the
564 early 1920s (McKenzie et al., 2009). Similarly, the invasive grass *Cenchrus ciliaris*
565 was well-established in some areas of the catchment by the 1960s. However, the
566 significant shift in sedimentation history recorded in the core at 14 Mile Pool does not
567 occur until several decades after the most intensive pastoral disturbances (Fig. A.1, 3).
568
569 *3.2.1.3. Period 3 (P3)— CE 700–1600: Lower interannual variability*
570 Accumulation rates in this period (49-61 cm; Fig. 3) were likely at least ten-fold
571 slower than P2 (i.e., 0.01 vs 0.07–0.1 $g \cdot cm^{-2} \cdot yr^{-1}$). When considered together with a
572 finer particle size (<2 mm), these findings suggest 14 Mile Pool experienced flood

573 events with relatively low to moderate energy that provided an ephemeral but
574 relatively reliable seasonal hydrology between CE 700–1600 (P3, Fig. 3). $\delta^{13}C$ of
575 total C was on average higher in P3 (+2.3 ‰) than in P2 although C and N contents
576 were not significantly different than from those of P2 (Fig. 3). The inclusion of
577 terrestrial plant and aquatic invertebrate (e.g., tadpole shrimp remains) macrofossils
578 for this record at ~ CE 700 also suggests a less dynamic environment than P1 and P2
579 and low primary production in the aquatic network and terrestrial catchment, or
580 transport of materials through regular runoff (Gayo et al., 2012). Our multi-proxy
581 record shows that these conditions persisted at the site until at least CE 1600 (Fig. 3).
582
583 *3.2.1.4. Period 4 (P4)—CE <100–700: Megadrought*
584 The heavily compacted, homogeneous and dry silts of the sediment profile were
585 underlain by a hard layer in the earliest section (48–61 cm), suggesting very low but
586 steady accumulation rates that are consistent with prolonged droughts, in the order of
587 decades to centuries (Fig. 3). Sediment total N and C contents were near or below
588 detection limits (0.01 and 0.4 %, respectively) during this period. Very low organic
589 matter (<0.4 % C) during this period indicates limited production, transport and/or
590 preservation of materials in the pool and catchment. This low OM and N content also
591 suggests the highest level of sub-aerial oxidation for the record, which we interpret as
592 indicative of regular and prolonged drying (Fig. 3). 14 Mile Pool at this time would
593 thus have been an episodic, clay pan-like system with a low-energy inundation regime.
594 The absence of suitable macrofossils for dating precluded estimation of the onset of
595 the core; tentative dating of bulk sediment samples also yielded incoherent age
596 estimates. We thus conservatively estimate the arid conditions inferred in the Upper
597 Fortescue River catchment to have spanned between CE <100 and 700 in the record

by extrapolating the age-depth models from P3. However, the age estimate extrapolated from Model 2 (Fig. 3) goes back as far as BCE 500, and together with the very dry, fine and compact lithology suggests that this record could be significantly older than estimated here. In addition, this period is likely to have been the most strongly affected by deflation creating hiatuses in the sequence due to the extremely dry conditions (Verschuren et al., 1999; Bristow et al., 2009), which could push back the onset even further towards the mid Holocene.

4. Discussion

4.1. Climate and environmental changes over the last ~2000 years

4.1.1. Period 1 (P1)—CE 1990 to present

The perennial aquatic depositional environment that we have reconstructed from the sediment indicators in P1 (post-1990) is consistent with regional instrumental rainfall data (Shi et al., 2008; Taschetto and England, 2009; Gallant and Karoly, 2010) and paleoclimatic reconstructions of increased rainfall (Cullen and Grierson, 2007; O'Donnell et al., 2015). Increased hydrological persistence of the 14 Mile Pool over the last 20 years could be explained by a wetter and more reliable (less variable) rainfall regime resulting in limited supraseasonal droughts. In particular, this pattern of wetter conditions is consistent with the significant increase in annual hot and wet extremes and decrease in cold and dry extremes over the last century in northwest Australia (Gallant and Karoly, 2010).

At the larger scale, current moisture delivery in the Australian tropics and subtropics is influenced by several different interacting modes of interannual climate variability (Risbey et al., 2009; Fierro and Leslie, 2013; Fredericksen et al., 2014; Fredericksen

623 and Grainger, 2015). Increased rainfall in northwest Australia in the late 1900s and
624 early 2000s compared to the last 100–200 years has been attributed to shifts in
625 cyclonic activity and tropical lows (Hassim and Walsh, 2008; Goebbert and Leslie,
626 2010; Lavender and Abbs, 2013; Kossin et al., 2014), and more broadly to an
627 anomalously positive Southern Annular Mode (SAM) (Fierro and Leslie, 2013;
628 Hendon et al., 2014; O'Donnell et al., 2015), enhanced La Niña conditions (Fierro
629 and Leslie, 2013) and also to the warming of the Tropical Western Pacific Warm Pool
630 (Lin and Li, 2012).
631
632 The southern annular mode (SAM), also referred to as the Antarctic Oscillation, has
633 been anomalously positive over the last 60 years (Villalba et al., 2012; Abrams et al.,
634 2013). A positive phase of the SAM usually results in drier conditions in southwest
635 and southeast Australia (Risbey et al., 2009); however, a positive phase of the SAM in
636 summer and autumn can also drive wetter conditions in the subtropics, particularly
637 northwest Australia. For example, Hendon et al., (2014) recently described the role of
638 positive phases of the SAM during summer and autumn in driving 'eddy-induced
639 divergent meridional circulation in the subtropics' and a poleward shift of the
640 subtropical dry zone, resulting in higher precipitation in the subtropics. The
641 significant link between the positive phase of the SAM and increased TC activity in
642 the northwest of Australia was attributed to enhanced humidity and ascending
643 motions (Mao et al., 2013). Interestingly, a recent tree-ring reconstruction from the
644 Pilbara has also revealed strong correlations between the SAM and tree growth as
645 well as with regional precipitation in summer and autumn (O'Donnell et al., 2015; Fig.
646 2b, c). Thus, a possible mechanism for the shift from P2 and P1 identified in the
647 sediment record is a more positive SAM in this period; we would also infer that this

influence of SAM was not as dominant in the previous 2000 years at least in the subtropical northwest.

4.1.2. Period 2 (P2)—CE 1600–1990

Collectively, the sedimentary evidence from the 14 Mile Pool suggests the P2 period was punctuated with one or multiple extreme flood(s) that would have been of much higher energy than any other period in the last ~2000 years. However, an overall increased rainfall for this period when compared to the most recent record (P1) is unlikely. Most of the events with sufficient intensity to cause the extreme floods are likely to originate from summer cyclonic rainfall (Rouillard et al., 2015). Hence conditions/drivers that would increase the genesis of TCs making land fall in the Pilbara likely peaked during at least one or more years. The onset of this period (P2) coincides with the onset of the LIA chronozone, where colder temperatures were recorded by high-resolution proxies between CE 1580 and 1880 in Australasia (PAGES 2k Consortium, 2013). Because the NH was colder still during the LIA, this period has been associated with a southward shift in the summer position of the ITCZ between CE 1400 and 1850 (Yancheva et al., 2007; Sachs et al., 2009; Tierney et al., 2010; Bird et al., 2011).

Under such a scenario, the rain belt of the ITCZ was likely pushed south of its modern position and many northern equatorial sites record extensive drought at that time (e.g., Sachs et al., 2009). The Pacific ITCZ is suggested to have been southward by as much as 5˚ during the LIA (Sachs et al., 2009). In the subtropical Pilbara, southward shifts or incursions might have been a primary force in bringing more intense TC rains in the summer (i.e., more southern location of TC genesis) that could have resulted in

673 the extreme floods recorded here. During the peak LIA, southward shift in the ITCZ
674 was inferred from 'wet' conditions observed south of contemporary summer
675 latitudinal position in Africa (e.g., Verschuren, 2004), South America (Haug et al.,
676 2001; Bird et al., 2011), the Pacific islands (Sachs et al., 2009) and (Indo-Pacific)
677 eastern Australia/Australasia (Tierney et al., 2010; Burrows et al., 2014) while
678 becoming drier northward. Though the influence of the ITCZ on rainfall has also been
679 suggested for other cool periods of the late Quaternary for these regions, spatial
680 inconsistencies in the African records have been identified from meta-analyses,
681 highlighting the complexity of climatic systems and non-linearity in the
682 environmental responses to hydroclimatic change and likely non-stationarity on
683 millennial timescales (Stager et al., 2011; Burrough and Thomas, 2013; Singarayer
684 and Burrough, 2015).
685
686 Most TCs that landfall in the Pilbara are formed off the coast within the ITCZ thanks
687 to favourable conditions brought together in the summer (Ramsay et al., 2012).
688 Extreme floods during the LIA might have also been caused by the interaction of a
689 more southern ITCZ (monsoonal trough) and strong La Niña events (Yan et al., 2011),
690 also associated with tropical cyclogenesis and particularly wet summers in the
691 northwest and northeast regions (Risbey et al., 2009; Goebbert and Leslie, 2010;
692 Ramsay et al., 2012; Chand et al., 2013). However, recent evidence suggested that the
693 MJO may have a more important role in TC genesis for this region compared to the
694 ENSO than previously recognised (Hall et al., 2001; Leroy and Wheeler, 2008;
695 Ramsay et al., 2012; Klotzbach, 2014; Klotzbach and Oliver, 2015). In particular, the
696 positive phase of the MJO has been associated with increased TC activity in the
697 southern Indian Ocean basin and along the northwest coast (Klotzbach and Oliver,

698 2015). In other basins, including the southwest Pacific, the MJO effects are typically
699 overcome by the ENSO, but no strong relationship has been established of the
700 combined effects of the MJO and ENSO on TCs for southern Indian Ocean basin
701 (Klotzbach and Oliver, 2015). This evidence suggests that while particularly intense
702 TCs in eastern Pilbara forming within a more southern ITCZ over the northwest coast
703 may have caused the extreme floods of P2, the role of interannual large scale drivers
704 of regional moisture delivery like the MJO may be underestimated.
705
706 Potentially contrasting evidence for our interpretation of P2 comes from the overall
707 drier conditions during the LIA chronozone compared to the last ~1000 years inferred
708 for a limited number of terrestrial records from the Australian tropics during the LIA
709 chronozone, which have recently been attributed to shifts in the ENSO rather than
710 migration of the the ITCZ (Denniston et al., 2015; Yan et al., 2015). Assuming peat
711 humification records indeed respond linearly to regional hydrological change rather
712 than local conditions (Burrows et al., 2014; Fig. 2), mean climatic state in the
713 northeast tropics of Australia may have been drier during the LIA chronozone (Yan et
714 al., 2015). Nevertheless, Burrows et al.'s study (2014) identified at least one
715 regionally coherent wet shift during this period that could have been registered in the
716 Fortescue Marsh record as extreme floods. Very few paleoecological records in
717 northwest Australia have detailed information for the last 1000 years to enable further
718 comparison (Yan et al., 2015; Fig. 2). Major peaks in fluvial activity on the millennial
719 scale have also been recorded for the last 300 years in the Black Spring sediment core,
720 collected inland in the Kimberley region (McGowan et al., 2012). The δ^{18}O-based
721 speleothem record from the Kimberley coast suggests that during the Holocene, the
722 Indonesian Australian summer monsoon (IASM) was at its lowest intensity (less

723 monsoonal rain) between 2000 and 1000 years ago, and has been strengthening in
724 intensity since (Denniston et al., 2013). In parallel, the 'mud layers' from the same
725 speleothem sequence have been associated with extreme rainfall events brought by
726 TCs suggesting reduced activity during CE 1450–1650 (Denniston et al., 2015). A
727 significant hiatus in these two speleothem records during the LIA chronozone
728 captured by the 14 Mile Pool core makes it difficult to assess further if reconstructed
729 hydroclimate variables reflected a mean climatic state for this period or the
730 occurrence of extremes such as the extreme floods. Our inferred extreme floods for
731 the CE 1600–1990 period (P2) would be, however, consistent with a period of
732 relatively high TC activity—with strong multidecadal variability—reconstructed
733 between CE 1600–1800 from a speleothem $\delta^{18}O$ record at Cape Range (northwest
734 Australia) and Chillagoe (northeast Australia) (Haig et al., 2014). The speleothem-
735 based index for TC activity developed at these locations was however, not correlated
736 to rainfall and showed the lowest values for the respective records post-1960 (~P1).
737
738 High spatial variability in hydroclimatic conditions both at present and in the past
739 across the vast tropical and sub-tropical region of Australia could also explain the
740 differences in interpretation among records (Risbey et al., 2009; Singarayer and
741 Burrough, 2015). For example, O'Donnell and al. (2015) showed that annual rainfall
742 patterns in the last century from the Upper Fortescue catchment were not strongly
743 correlated to the coastal rainfall regime of the Pilbara (i.e., Cape Range), nor with the
744 broader tropics (Fig. 2b). Similarly, the development of additional late Holocene
745 records of hydroclimatic conditions in summer rainfall dominated Africa is
746 suggesting a higher spatial heterogeneity than previously thought (e.g., Stager et al.,
747 2013; Woodborne et al., 2015). This disparity between periods and records in the

748 northwest could also be explained by summertime rainfall being influenced by spatial
749 shifts (i.e., more inland) in the tracks of the landfalling TCs and of other synoptic
750 weather patterns (Berry et al., 2011; Ramsey et al., 2012), and/or that regional
751 moisture delivery and dominant sources are influenced by the interaction between
752 multiple large-scale forcing mechanisms discussed previously (Frederiksen and
753 Grainger, 2015).
754
755 *4.1.3. Period 3 (P3)—CE 700–1600*
756 The relatively less intense but less variable hydrology (although drier overall than P1
757 and P2) from circa CE 700 in P3 is consistent with records showing a shift to
758 decreased aridity at the onset of this period from the mid-Holocene between CE 700–
759 1100 in the tropical north-west of Australia (McGowan et al., 2012; Fig. 2). As
760 previously discussed, the relatively 'wet' conditions in the tropical north of the region
761 during this period have been attributed to a progressive strengthening of the IASM
762 post ~CE 1050 enabled by a weakening of the ENSO (Denniston et al., 2013). The
763 weakening of the ENSO was consistent with TCs increasing, which could explain
764 higher rainfall in the system (Nicholls, 1992). However, the monsoonal system acting
765 as a primary mechanism for the delivery of moisture over the Pilbara at that time—as
766 opposed to TCs—is consistent with the more northern position of the ITCZ
767 (Yancheva et al., 2007; Sachs et al., 2009; PAGES 2k Consortium, 2013).
768
769 Our results show that CE 700–1600 (P3) was a prolonged period characterised by less
770 vigorous but regular flows, episodically inundating a more ephemeral aquatic
771 environment. Sediment at a site ~1000 km to the northeast of the Fortescue Marsh in
772 the eastern Kimberley region (#5, Fig. 2a), also revealed a rapid increase in fluvial

773 sedimentation around CE 650–850 concurrent with a more progressive increase in
774 woody vegetation characteristic of the modern composition (McGowan et al., 2012).
775 Recent analysis of speleothems from the Kimberley region and from Indonesia also
776 shows that relatively wet conditions during the late Holocene was established
777 following a relatively sharp transition between CE 750–1050 (Denniston et al., 2013).
778 Consequently, the onset of relatively wetter conditions in the late Holocene from P3
779 at the 14 Mile Pool may have been linked to a change in hydroclimatic regime
780 affecting the tropics and subtropics similarly.
781
782 This shift in regional climate of the northwest from ~CE 700 further appears to have
783 been quite widespread in the Australian arid zone. For example, in central Australia
784 (Northern Territory), extreme floods at the Ross River were recorded to have been
785 more frequent during the late Holocene (i.e., CE 450–1250; Patton et al., 1993).
786 Lower dust emissions (i.e., less dry) from the Lake Eyre Basin at CE 1100 were also
787 attributed to a decrease in climate variability (decrease in ENSO activity), though
788 concurrent change in aridity was not clear (Marx et al., 2009). Climatic amelioration
789 and enhanced growth of vegetation in the arid zone is also reflected by a wealth of
790 evidence from the archaeological literature supporting models of increased regional
791 occupation between ~CE 500–1000 (Smith and Ross, 2008; Smith et al., 2008;
792 McDonald and Veth, 2013; Williams, 2013; Williams et al., 2015).
793
794 *4.1.4 Period 4 (P4)—CE <100–700*
795 The hyperarid conditions inferred in P4 appear quite coherent throughout the
796 Australian arid zones from ~5000 calibrated years before present (cal yrs BP) (Marx
797 et al., 2009; Denniston et al., 2013; Reeves et al., 2013a, b). The analysis of a 6500-

year long record of combined pollen and aeolian dust from the Kimberley region revealed a ‘megadrought' (~1500 years long) had been ongoing in the Australian northwest since 2400 cal yrs BP/ CE −450 (McGowan et al., 2012; Fig. 2). Less frequent and shorter-lived wet shifts were identified in the northeast tropics from peat humification records prior to ~ CE 500 (Burrows et al., 2014). These studies support conclusions from early work on the formation of cheniers and sand dunes from northern Australian tropical rivers, which also identified a particularly dry period during the 2800–1600 cal yrs BP/ CE −850 to 350, with suggestions that this could be as early as 3800 cal yrs BP/ CE −1850 (Lees 1992; Shulmeister and Lees, 1995). The evidence included wide-ranging declines in effective precipitation, lake levels (Shulmeister and Lees, 1995) and fluvial discharge (Lees, 1992). Increasingly arid conditions from the mid-Holocene to ~1500 years ago in the northwest were also recently corroborated from a multi-proxy investigation of deep-sea sediment off the Pilbara coast (De Deckker et al., 2014), coastal Kimberley sediment (Proske et al., 2014), and from multiple Australasian speleothem records (Denniston et al., 2013), confirming that drought was widespread across the region. This aridification across northern Australia has been linked to particularly strong ENSO cycles and related failure of the monsoonal system, resulting in enhanced climatic variability (Denniston et al., 2013; De Deckker et al., 2014).

5. Conclusions

This study provides the first sedimentological evidence from the Pilbara revealing major hydrological changes have taken place in the arid subtropics of northwest Australia over the last 2000 years, including phases of extremely wet conditions (resulting from extreme floods) as well as an extended drought more than 1000 years

823 ago. The paleolimnological reconstruction for the most recent ~20 years is consistent
824 with the instrumental record, with 14 Mile Pool—the most regularly inundated pool
825 of the Fortescue Marsh today—becoming near perennial for what appears the first
826 time in the record. Importantly, the sediment stratigraphy reveals that extreme floods
827 occurred in the period CE 1600–1990, which is broadly synchronous with the LIA
828 chronozone. The results from our reconstruction are consistent with other records of
829 wetter climes or at least of high intensity wet peaks for the SH that have been linked
830 to a southward shift in the ITCZ and/or more pervasive La Niña-like conditions, but
831 may also be more specifically due to the influence of other regional hydroclimatic
832 drivers on tropical cyclogenesis such as the MJO. For the earlier sections of the
833 sedimentary sequence, we show that the eastern Pilbara responded until circa CE 700
834 to a megadrought pervasive in most of the Australian arid zone and originating in the
835 mid Holocene, which was followed by climatic amelioration likely related to
836 weakening of the ENSO and strengthening of monsoonal patterns. The results suggest
837 that the dominant forcing mechanisms of moisture delivery on the arid northwest
838 Australian landscape have not been stationary over the last 2000 years.
839
840 Overall, we show that the increased seasonality of rainfall over the last 2000 years
841 was experienced in the Marsh with the catchment becoming ‘wetter’ (increasing the
842 recharge), demonstrating the importance of establishing the variability of a system
843 and not just its long-term average climatic conditions. We suggest that the increased
844 difference among paleohydrological records from the northwest, northern tropics and
845 northeast tropical and sub-tropical Australian regions during the late Holocene may
846 have been due to non-stationarity in the strength of large-scale forcing mechanisms on
847 TC genesis location, direction of tracks, frequency and intensity (through ITCZ,

ENSO, MJO and/or SAM). Further work developing paleohydrological records from the Australian tropics and sub-tropics is crucial for refining our understanding of these competing modes of variability and their likely behaviour under future scenarios. By providing a baseline of hydrological change, the findings from our study have implications for exploring past and potential future changes in the drivers of moisture in subtropical drylands. These results also provide a window for appraising how water-limited ecosystems that have proved resilient through significant shifts in hydrology over the recent past might cope with increasing land-use pressures and/or altered hydrological variability in the future.

Acknowledgements

We thank David Thomas (Oxford University), Dirk Verschuren (Ghent University) and John Tibby (University of Adelaide) for their thorough and constructive comments on an early draft as well as our two anonymous reviewers, which have helped focus and improve the quality of the paper. We also thank Charlotte Cook (UNSW) and John Tibby for pollen and diatom assessments. This research was supported by the Australian Research Council in partnership with Rio Tinto (LP120100310) and AINSE grant ALNGRA13043. A. Rouillard was supported by an International Postgraduate Research Scholarship (IPRS), an Australian Postgraduate Award (APA), and Natural Sciences and Engineering Research Council (NSERC) and Fonds québécois de la recherche sur la nature et les technologies (FQRNT) graduate scholarships. G. Skrzypek was supported by an ARC Future Fellowship (FT110100352). We thank Glenn Kirkpatrick, Douglas Ford, Ray Scott and Bill Wilson for field and technical support. We are grateful to Fortescue Metals Group Ltd for providing access to ortho-imagery, digital elevation model (DEM) and field sites. The high-resolution dry image of the core was provided by the Geological Survey of Western Australia. We also acknowledge the kind field support of Murray and Ray Kennedy (Roy Hill Station), Sue and Lee Bickell (Marillana Station), Barry and Bella Grett (Ethel Creek Station) and Victor and Larissa Gleeson (Mulga Downs Station). We thank Charlotte Cook (UNSW) and John Tibby (Uni. Adelaide) for preliminary assessment of pollen and diatom samples. Screening for chironomids and identification was kindly conducted by Wetland Resources Management (Perth, Australia). Patrick De Deckker (ANU) and Stuart Halse (Bennelongia Pty Ltd) helped with early ostracod identification and Todd Erickson (UWA) provided seed identification. We also thank Gavan McGrath, Nik Callow (UWA), Caroline Bird

882 (Archae-Aus), Simon Haberle (ANU), Jonathan Palmer (UNSW), Adrienne Marquis
883 (DPaW) for their useful and generous advice.
884

885 **References**

886 Abram NJ, Mulvaney R, Vimeux F, Phipps SJ, Turner J, England MH (2014)
887 Evolution of the Southern Annular Mode during the past millennium. Nature
888 Climate Change 4:564–569
889 Adair EC, Burke IC (2010) Plant phenology and life span influence soil pool
890 dynamics: *Bromus tectorum* invasion of perennial C_3-C_4 grass communities.
891 Plant Soil 335:255–269
892 Appleby PG (2001) Chronostratigraphic techniques in recent sediments. In: Last WM,
893 Smol JP (eds) Volume 1: Basin Analysis, Coring, and Chronological
894 Techniques. Springer, Dordrecht, pp 171-203
895 Baird W (1843) Notes on the British Entomostraca. Zoologist 1:193–197
896 Battin TJ, Kaplan LA, Findlay S, Hopkinson CS, Marti E, Packman AI, Newbold JD,
897 Sabater F (2008) Biophysical controls on organic carbon fluxes in fluvial
898 networks. Nature Geoscience 1:95–100
899 Beard JS (1975) The Vegetation of the Pilbara Area, Vegetation Survey of Western
900 Australia, 1: 1000000 Vegetation Series, Map and Explanatory Notes. The
901 University of Western Australia Press, Nedlands
902 Berry G, Reeder MJ, Jakob C (2011) Physical mechanisms regulating summertime
903 rainfall over northwestern Australia. Journal of Climate 24:3705–3717
904 Bessems I, Verschuren D, Russell JM, Hus J, Mees F, Cumming BF (2008)
905 Palaeolimnological evidence for widespread late 18th century drought across

906 equatorial East Africa. Palaeogeography, Palaeoclimatology, Palaeoecology
907 259:107–120
908 Bird BW, Abbott MB, Vuille M, Rodbell DT, Stansell ND, Rosenmeier MF (2011) A
909 2,300-year-long annually resolved record of the South American summer
910 monsoon from the Peruvian Andes. Proceedings of the National Academy of
911 Sciences 108:8583–8588
912 Björck S, Wohlfarth B (2001) ^{14}C chronostratigraphic techniques in paleolimnology.
913 In: Last WM, Smol JP (eds) Volume 1: Basin Analysis, Coring, and
914 Chronological Techniques. Springer, Dordrecht, 205–245
915 Blaauw M (2010) Methods and code for 'classical' age-modelling of radiocarbon
916 sequences. Quaternary Geochronology 5:512–518
917 Blott SJ, Pye K (2001) GRADISTAT: a grain size distribution and statistics package
918 for the analysis of unconsolidated sediments. Earth surface processes and
919 Landforms 26:1237–1248
920 Brahney J, Ballantyne AP, Turner BL, Spaulding SA, Otu M, Neff JC (2014)
921 Separating the influences of diagenesis, productivity and anthropogenic nitrogen
922 deposition on sedimentary $\delta^{15}N$ variations. Organic Geochemistry 75:140–150
923 Brenner M, Whitmore TJ, Curtis JH, Hodell DA, Schelske CL (1999) Stable isotope
924 ($\delta^{13}C$ and $\delta^{15}N$) signatures of sedimented organic matter as indicators of historic
925 lake trophic state. Journal of Paleolimnology 22:205–221
926 Bristow CS, Drake N, Armitage S (2009) Deflation in the dustiest place on Earth: the
927 Bodélé Depression, Chad. Geomorphology 105:50–58
928 Broccoli AJ, Dahl KA, Stouffer RJ (2006) Response of the ITCZ to Northern
929 Hemisphere cooling. Geophysical Research Letters 33

930 Brodie CR, Casford JSL, Lloyd JM, Leng MJ, Heaton THE, Kendrick CP, Yongqiang
931 Z (2011) Evidence for bias in C/N, δ^{13}C and δ^{15}N values of bulk organic matter,
932 and on environmental interpretation, from a lake sedimentary sequence by pre-
933 analysis acid treatment methods. Quaternary Science Reviews 30:3076–3087
934 Bronk Ramsey C (2008) Deposition models for chronological records. Quaternary
935 Science Reviews 27:42–60
936 Bronk Ramsey C (2009) Bayesian analysis of radiocarbon dates. Radiocarbon
937 51:337–360
938 Burrough SL, Thomas DSG (2013) Central southern Africa at the time of the African
939 Humid Period: a new analysis of Holocene palaeoenvironmental and
940 palaeoclimate data. Quaternary Science Reviews 80:29–46
941 Burrows MA, Fenner J, Haberle SG (2014) Humification in northeast Australia:
942 Dating millennial and centennial scale climate variability in the late Holocene.
943 The Holocene 1–12
944 Chand SS, Tory KJ, McBride JL, Wheeler MC, Dare RA, Walsh KJE (2013) The
945 different impact of positive-neutral and negative-neutral ENSO regimes on
946 Australian tropical cyclones. Journal of Climate 26:8008–8016
947 Coianiz L, Ariztegui D, Piovano EL, Lami A, Guilizzoni P, Gerli S, Waldmann N
948 (2015) Environmental change in subtropical South America for the last two
949 millennia as shown by lacustrine pigments. Journal of Paleolimnology 53:233–
950 250
951 Cullen LE, Grierson PF (2007) A stable oxygen, but not carbon, isotope chronology
952 of Callitris columellaris reflects recent climate change in north-western
953 Australia. Climatic Change 85:213–229

954 Cuna E, Zawisza E, Caballero M, Ruiz-Fernández AC, Lozano-García S, Alcocer J
955 (2014) Environmental impacts of Little Ice Age cooling in central Mexico
956 recorded in the sediments of a tropical alpine lake. Journal of Paleolimnology
957 51:1–14
958 Dare RA, Davidson NE, McBride JL (2012) Tropical cyclone contribution to rainfall
959 over Australia. Monthly Weather Review 140:3606–3619
960 De Deckker P, Barrows TT, Rogers J (2014) Land-sea correlations in the Australian
961 region: post-glacial onset of the monsoon in northwestern Western Australia.
962 Quaternary Science Reviews 105:181–194
963 Denniston RF, Villarini G, Gonzales AN, Wyrwoll K-H, Polyak VJ, Ummenhofer CC,
964 Lachniet MS, Wanamaker AD, Humphreys WF, Woods D, others (2015)
965 Extreme rainfall activity in the Australian tropics reflects changes in the El
966 Niño/Southern Oscillation over the last two millennia. Proceedings of the
967 National Academy of Sciences 112:4576–4581
968 Denniston RF, Wyrwoll K-H, Polyak VJ, Brown JR, Asmerom Y, Wanamaker J,
969 Alan D, LaPointe Z, Ellerbroek R, Barthelmes M, Cleary D, others (2013) A
970 Stalagmite record of Holocene Indonesian-Australian summer monsoon
971 variability from the Australian tropics. Quaternary Science Reviews 78:155–168
972 Department of Lands and Surveys (1892) 1892–94 North West [Tally No. 505580].
973 Cancelled Public Plans 1878–1907 (Standard Series), State Records Office of
974 Western Australia (SROWA) Acc 541. Available from:
975 <http://aeon.sro.wa.gov.au> [8 April 2015]
976 Department of Lands and Surveys (1894) 1894 North West [Tally No. 505581].
977 Cancelled Public Plans 1878–1907 (Standard Series), State Records Office of

Western Australia (SROWA) Acc 541. Available from: <http://aeon.sro.wa.gov.au> [8 April 2015]

Department of Lands and Surveys (1899) 1899–1905 North West [Tally No. 505582]. Cancelled Public Plans 1878–1907 (Standard Series), State Records Office of Western Australia (SROWA) Acc 541. Available from: <http://aeon.sro.wa.gov.au> [8 April 2015]

Department of Lands and Surveys (1905a) 1905–05 300 Chain Plan [Tally No. 503157]. Cancelled Public Pans 1903–1965 (Original State Series; 300 Chain Plans), State Records Office of Western Australia (SROWA) Acc 541. Available from: <http://aeon.sro.wa.gov.au> [8 April 2015]

Department of Lands and Surveys (1905b) 1905–09 300 Chain Plan [Tally No. 503158]. Cancelled Public Pans 1903–1965 (Original State Series; 300 Chain Plans), State Records Office of Western Australia (SROWA) Acc 541. Available from: <http://aeon.sro.wa.gov.au> [8 April 2015]

Department of Lands and Surveys (1909) 1909–16 300 Chain Plan [Tally No. 503159]. Cancelled Public Pans 1903–1965 (Original State Series; 300 Chain Plans), State Records Office of Western Australia (SROWA) Acc 541. Available from: <http://aeon.sro.wa.gov.au> [8 April 2015]

Department of Lands and Surveys (1919) File 1919/05125: Letter Athol J. Bennett to Surveyor General, 05/09/1919. Surveys by Roy Hill Pastoral Co in Victoria district of Roy Hill Station, Folio 13, State Records Office of Western Australia (SROWA) Acc 541

Department of Lands and Surveys (1921) 1921–24 300 Chain Plan [Tally No. 503161]. Cancelled Public Pans 1903–1965 (Original State Series; 300 Chain

1002 Plans), State Records Office of Western Australia (SROWA) Acc 541.
1003 Available from: <http://aeon.sro.wa.gov.au> [8 April 2015]
1004 Department of Lands and Surveys (1924) 1924–29 300 Chain Plan [Tally No.
1005 503162]. Cancelled Public Pans 1903–1965 (Original State Series; 300 Chain
1006 Plans), State Records Office of Western Australia (SROWA) Acc 541.
1007 Available from: <http://aeon.sro.wa.gov.au> [8 April 2015]
1008 Department of Lands and Surveys (1952) 1952–61 300 Chain Plan [Tally No.
1009 503164]. Cancelled Public Pans 1903–1965 (Original State Series; 300 Chain
1010 Plans), State Records Office of Western Australia (SROWA) Acc 541.
1011 Available from: <http://aeon.sro.wa.gov.au> [8 April 2015]
1012 Donselaar ME, Gozalo C, Moyano S (2013) Avulsion processes at the terminus of
1013 low-gradient semi-arid fluvial systems: Lessons from the Río Colorado,
1014 Altiplano endorheic basin, Bolivia. Sedimentary Geology 283:1–14
1015 Dunne T, Western D, Dietrich WE (2011) Effects of cattle trampling on vegetation,
1016 infiltration, and erosion in a tropical rangeland. Journal of Arid Environments
1017 75:58–69
1018 Eldridge DJ, Koen TB, Killgore A, Huang N, Whitford WG (2012) Animal foraging
1019 as a mechanism for sediment movement and soil nutrient development: evidence
1020 from the semi-arid Australian woodlands and the Chihuahuan Desert.
1021 Geomorphology 157:131–141
1022 Fierro AO, Leslie LM (2013) Links between Central West Western Australian
1023 Rainfall Variability and Large-Scale Climate Drivers. Journal of Climate
1024 26:2222–2245
1025 Fink D, Hotchkis M, Hua Q, Jacobsen G, Smith AM, Zoppi U, Child D, Mifsud C,
1026 van dG, Haitse, Williams A, others (2004) The ANTARES AMS facility at

ANSTO. Nuclear Instruments and Methods in Physics Research Section B: Beam Interactions with Materials and Atoms 223:109–115

Finlay JC, Kendall C (2008) Stable isotope tracing of temporal and spatial variability in organic matter sources to freshwater ecosystems. In: Michener R, Lajtha K (eds) Stable isotopes in ecology and environmental science. Wiley-Blackwell, Hoboken, Oxford, UK, 283–333

Fitzsimmons KE, Cohen TJ, Hesse PP, Jansen J, Nanson GC, May J-H, Barrows TT, Haberlah D, Hilgers A, Kelly T, others (2013) Late Quaternary palaeoenvironmental change in the Australian drylands. Quaternary Science Reviews 74:78–96

Frederiksen CS, Grainger S (2015) The role of external forcing in prolonged trends in Australian rainfall. Climate Dynamics 1–14 DOI: 10.1007/s00382-015-2482-8

Frederiksen CS, Zheng X, Grainger S (2014) Teleconnections and predictive characteristics of Australian seasonal rainfall. Climate Dynamics 43:1381–1408

Ford DJ, Cookson WR, Adams MA, Grierson PF (2007) Role of soil drying in nitrogen mineralization and microbial community function in semi-arid grasslands of north-west Australia. Soil Biology and Biochemistry 39:1557–1569

Gallant AJE, Karoly DJ (2010) A combined climate extremes index for the Australian region. Bulletin of the American Meteorological Society

Gälman V, Rydberg J, Bigler C (2009) Decadal diagenetic effects on $\delta^{13}C$ and $\delta^{15}N$ studied in varved lake sediment. Limnology and Oceanography 54:917–924

Gayo EM, Latorre C, Santoro CM, Maldonado A, De Pol-Holz R (2012) Hydroclimate variability in the low-elevation Atacama Desert over the last 2500 yr. Climate of the Past 8:287–306

1052 Gell PA, Bulpin S, Wallbrink P, Hancock G, Bickford S (2005) Tareena Billabong - a
1053 palaeolimnological history of an ever-changing wetland, Chowilla Floodplain,
1054 lower Murray-Darling basin, Australia. Marine and Freshwater Research
1055 56:441–456
1056 Goebbert KH, Leslie LM (2010) Interannual variability of Northwest Australian
1057 tropical cyclones. Journal of Climate 23:4538–4555
1058 Graham NE, Ammann CM, Fleitmann D, Cobb KM, Luterbacher J (2011) Support
1059 for global climate reorganization during the "Medieval Climate Anomaly".
1060 Climate Dynamics 37:1217–1245
1061 Haig J, Nott J, Reichart G-J (2014) Australian tropical cyclone activity lower than at
1062 any time over the past 550-1,500 years. Nature 505:667–671
1063 Hall JD, Matthews AJ, Karoly DJ (2001) The modulation of tropical cyclone activity
1064 in the Australian region by the Madden-Julian Oscillation. Monthly Weather
1065 Review 129:2970–2982
1066 Hassim MEE, Walsh KJE (2008) Tropical cyclone trends in the Australian region.
1067 Geochemistry, Geophysics, Geosystems 9
1068 Haug GH, Hughen KA, Sigman DM, Peterson LC, Röhl U (2001) Southward
1069 migration of the intertropical convergence zone through the Holocene. Science
1070 293:1304–1308
1071 Hendon HH, Lim E-P, Nguyen H (2014) Seasonal variations of subtropical
1072 precipitation associated with the southern annular mode. Journal of Climate
1073 27:3446–3460
1074 Hesse PP, Magee JW, van der Kaars S (2004) Late Quaternary climates of the
1075 Australian arid zone: a review. Quaternary International 118:87–102

1076 Hodell DA, Brenner M, Curtis JH, Medina-González R, Can EI-C, Albornaz-Pat A,
1077 Guilderson TP (2005) Climate change on the Yucatan Peninsula during the
1078 Little Ice Age. Quaternary Research 63:109–121
1079 Hogg AG, Hua Q, Blackwell PG, Niu M, Buck CE, Guilderson TP, Heaton TJ,
1080 Palmer JG, Reimer PJ, Reimer RW, others (2013) SHCal13 Southern
1081 Hemisphere calibration, 0-50,000 cal yr BP. Radiocarbon 55:1889–1903
1082 Hua Q, Jacobsen GE, Zoppi U, Lawson EM, Williams AA, Smith AM, McGann MJ
1083 (2001) Progress in radiocarbon target preparation at the ANTARES AMS
1084 Centre. Radiocarbon 43:275–282
1085 Hua Q, Barbetti M, Rakowski AZ (2013) Atmospheric radiocarbon for the period
1086 1950-2010. Radiocarbon 55: 2059–2072.
1087 Jenkins KM, Boulton AJ (2003) Connectivity in a dryland river: short-term aquatic
1088 microinvertebrate recruitment following floodplain inundation. Ecology
1089 84:2708–2723
1090 Jones LS, Schumm SA (2009) Causes of avulsion: an overview. Fluvial
1091 sedimentology VI 171–178
1092 Karanovic I (2008) Three interesting Cyprididae (Ostracoda) from Western Australia.
1093 Records of the Western Australian Museum 24:267–287
1094 Klotzbach PJ (2014) The Madden-Julian Oscillation's impacts on worldwide tropical
1095 cyclone activity. Journal of Climate 27:2317–2330
1096 Klotzbach PJ, Oliver ECJ (2015) Variations in Global Tropical Cyclone Activity and
1097 the Madden-Julian Oscillation Since the Mid-20th Century. Geophysical
1098 Research Letters 42:4199–4207
1099 Kossin JP, Emanuel KA, Vecchi GA (2014) The poleward migration of the location
1100 of tropical cyclone maximum intensity. Nature 509:349–352

1101 Lavender SL, Abbs DJ (2013) Trends in Australian rainfall: contribution of tropical
1102 cyclones and closed lows. Climate Dynamics 40:317–326
1103 Lees BG (1992) Geomorphological evidence for late Holocene climatic change in
1104 northern Australia. The Australian Geographer 23:1–10
1105 Leroy A, Wheeler MC (2008) Statistical prediction of weekly tropical cyclone
1106 activity in the Southern Hemisphere. Monthly Weather Review 136:3637–3654
1107 Leslie C, Hancock GJ (2008) Estimating the date corresponding to the horizon of the
1108 first detection of 137Cs and 239+ 240Pu in sediment cores. Journal of
1109 Environmental Radioactivity 99:483–490
1110 Lin Z, Li Y (2012) Remote influence of the tropical Atlantic on the variability and
1111 trend in North West Australia summer rainfall. Journal of Climate 25:2408–
1112 2420
1113 Mao R, Gong D-Y, Yang J, Zhang Z-Y, Kim S-J, He H-Z (2013) Is there a linkage
1114 between the tropical cyclone activity in the southern Indian Ocean and the
1115 Antarctic Oscillation? Journal of Geophysical Research: Atmospheres
1116 118:8519–8535
1117 Marx SK, Kamber BS, McGowan HA, Denholm J (2011) Holocene dust deposition
1118 rates in Australia's Murray-Darling Basin record the interplay between aridity
1119 and the position of the mid-latitude westerlies. Quaternary Science Reviews
1120 30:3290–3305
1121 Marx SK, McGowan HA, Kamber BS (2009) Long-range dust transport from eastern
1122 Australia: A proxy for Holocene aridity and ENSO-type climate variability.
1123 Earth and Planetary Science Letters 282:167–177
1124 Masson-Delmotte, V., M. Schulz, A. Abe-Ouchi, J. Beer, A. Ganopolski, J.F.
1125 González Rouco, E. Jansen, K. Lambeck, J. Luterbacher, T. Naish, T. Osborn, B.

1126 Otto-Bliesner, T. Quinn, R. Ramesh, M. Rojas, X. Shao, Timmermann A (2013)
1127 Information from Paleoclimate Archives. In: Stocker T, Qin D, Plattner G-K,
1128 Tignor M, Allen SK, Boschung J, Nauels A, Xia Y, Bex V, Midgley PM (eds)
1129 Climate Change 2013: The Physical Science Basis. Contribution of Working
1130 Group I to the Fifth Assessment Report of the Intergovernmental Panel on
1131 Climate Change. Cambridge University Press, Cambridge, UK, and New York,
1132 383–464
1133 McBride JL, Keenan TD (1982) Climatology of tropical cyclone genesis in the
1134 Australian region. Journal of Climatology 2:13–33
1135 McDonald J, Veth P (2013) Rock art in arid landscapes: Pilbara and Western Desert
1136 petroglyphs. Australian Archaeology 66
1137 McGowan H, Marx S, Moss P, Hammond A (2012) Evidence of ENSO mega-drought
1138 triggered collapse of prehistory Aboriginal society in northwest Australia.
1139 Geophysical Research Letters 39
1140 McIntyre RES, Adams MA, Ford DJ, Grierson PF (2009a) Rewetting and litter
1141 addition influence mineralisation and microbial communities in soils from a
1142 semi-arid intermittent stream. Soil Biology and Biochemistry 41:92–101
1143 McIntyre RES, Adams MA, Grierson PF (2009b) Nitrogen mineralization potential in
1144 rewetted soils from a semi-arid stream landscape, north-west Australia. Journal
1145 of Arid Environments 73:48–54
1146 McKenzie NL, van Leeuwen S, Pinder AM (2009) Introduction to the Pilbara
1147 biodiversity survey, 2002-2007. Records of the Western Australian Museum,
1148 Supplement 78:3–89

1149 Mohtadi M, Prange M, Oppo DW, De P-H, Ricardo, Merkel U, Zhang X, Steinke S,
1150 Lückge A (2014) North Atlantic forcing of tropical Indian Ocean climate.
1151 Nature 509:76–80
1152 Neukom R, Gergis J (2012) Southern Hemisphere high-resolution palaeoclimate
1153 records of the last 2000 years. The Holocene 22:501–524
1154 Ng B, Walsh K, Lavender S (2015) The contribution of tropical cyclones to rainfall in
1155 northwest Australia. International Journal of Climatology 35:2689–2697
1156 Nicholls N (1992) Recent performance of a method for forecasting Australian
1157 seasonal tropical cyclone activity. Australian Meteorological Magazine 40:105–
1158 110
1159 O'Donnell AJ, Cook ER, Palmer JG, Turney CSM, Page GFM, Grierson PF (2015)
1160 Tree Rings Show Recent High Summer-Autumn Precipitation in Northwest
1161 Australia Is Unprecedented within the Last Two Centuries. PloS one
1162 10:e0128533
1163 PAGES 2k Consortium: Ahmed M, Anchukaitis KJ, Asrat A, Borgaonkar HP, Braida
1164 M, Buckley BM, Büntgen U, Chase BM, Christie DA, Cook ER, Curran MAJ,
1165 Diaz HF, Esper J, Fan Z-X, Gaire NP, Ge Q, Gergis J, González-Rouco JF,
1166 Goosse H, Grab SW, Graham N, Graham R, Grosjean M, Hanhijärvi ST,
1167 Kaufman DS, Kiefer T, Kimura K, Korhola AA, Krusic PJ, Lara A, Lézine A-M,
1168 Ljungqvist FC, Lorrey AM, Luterbacher J, Masson-Delmotte V, McCarroll D,
1169 McConnell JR, McKay NP, Morales MS, Moy AD, Mulvaney R, Mundo IA,
1170 Nakatsuka T, Nash DJ, Neukom R, Nicholson SE, Oerter H, Palmer JG, Phipps
1171 SJ, Prieto MR, Rivera A, Sano M, Severi M, Shanahan TM, Shao X, Shi F, Sigl
1172 M, Smerdon JE, Solomina ON, Steig EJ, Stenni B, Thamban M, Trouet V,
1173 Turney CSM, Umer M, van Ommen T, Verschuren D, Viau AE, Villalba R,

1174 Vinther BM, von Gunten L, Wagner S, Wahl ER, Wanner H, Werner JP, White
1175 JWC, Yasue K, Zorita E (2013) Continental-scale temperature variability during
1176 the past two millennia. Nature Geoscience 6:339–346
1177 Palmer JG, Cook ER, Turney CSM, Allen K, Fenwick P, Cook BI, O'Donnell A,
1178 Lough J, Grierson P, Baker P (2015) Drought variability in the eastern Australia
1179 and New Zealand summer drought atlas (ANZDA, CE 1500-2012) modulated
1180 by the Interdecadal Pacific Oscillation. Environmental Research Letters
1181 10:124002
1182 Patton PC, Pickup G, Price DM (1993) Holocene paleofloods of the Ross River,
1183 central Australia. Quaternary Research 40:201–212
1184 Powell DM (2009) Dryland rivers: processes and forms. In: Parsons AJ, Abrahams
1185 AD (eds) Geomorphology of Desert Environments. Springer, pp 333-373
1186 Proske U, Heslop D, Haberle S (2014) A Holocene record of coastal landscape
1187 dynamics in the eastern Kimberley region, Australia. Journal of Quaternary
1188 Science 29:163–174
1189 Radke LC, Juggins S, Halse SA, De D, P, Finston T (2003) Chemical diversity in
1190 south-eastern Australian saline lakes II: biotic implications. Marine and
1191 Freshwater Research 54:895–912
1192 Ralph TJ, Kobayashi T, Garcia A, Hesse PP, Yonge D, Bleakley N, Ingleton T (2011)
1193 Paleoecological responses to avulsion and floodplain evolution in a semiarid
1194 Australian freshwater wetland. Australian Journal of Earth Sciences 58:75–91
1195 Ramsay HA, Camargo SJ, Kim D (2012) Cluster analysis of tropical cyclone tracks in
1196 the Southern Hemisphere. Climate Dynamics 39:897–917

1197 Reaney SM (2008) The use of agent based modelling techniques in hydrology:
1198 determining the spatial and temporal origin of channel flow in semi-arid
1199 catchments. Earth Surface Processes and Landforms 33:317–327
1200 Reeves JM, Bostock HC, Ayliffe LK, Barrows TT, Deckker PD, Devriendt LS,
1201 Dunbar GB, Drysdale RN, Fitzsimmons KE, Gagan MK, Griffiths ML, Haberle
1202 SG, Jansen JD, Krause C, Lewis S, McGregor HV, Mooney SD, Moss P,
1203 Nanson GC, Purcell A, van der Kaars S (2013a) Palaeoenvironmental change in
1204 tropical Australasia over the last 30,000 years—A synthesis by the OZ-
1205 INTIMATE group. Quaternary Science Reviews 74:97–114
1206 Reeves JM, Barrows TT, Cohen TJ, Kiem AS, Bostock HC, Fitzsimmons KE, Jansen
1207 JD, Kemp J, Krause C, Petherick L, Phipps SJ, OZ-INTIMATE Members
1208 (2013b) Climate variability over the last 35,000 years recorded in marine and
1209 terrestrial archives in the Australian region: an OZ-INTIMATE compilation.
1210 Quaternary Science Reviews 74:21–34
1211 Risbey JS, Pook MJ, McIntosh PC, Wheeler MC, Hendon HH (2009) On the remote
1212 drivers of rainfall variability in Australia. Monthly Weather Review 137:3233–
1213 3253
1214 Rouillard A, Skrzypek G, Dogramaci S, Turney C, Grierson PF (2015) Impacts of
1215 high inter-annual variability of rainfall on a century of extreme hydrologic
1216 regime of northwest Australia. Hydrology and Earth System Sciences 19:2057–
1217 2078
1218 Sachs JP, Sachse D, Smittenberg RH, Zhang Z, Battisti DS, Golubic S (2009)
1219 Southward movement of the Pacific intertropical convergence zone AD 1400--
1220 1850. Nature Geoscience 2:519–525

1221 Schelske CL, Peplow A, Brenner M, Spencer CN (1994) Low-background gamma
1222 counting: applications for 210 Pb dating of sediments. Journal of
1223 Paleolimnology 10:115–128
1224 Schidlowski M (1987) Application of stable carbon isotopes to early biochemical
1225 evolution on Earth. Annual Review of Earth and Planetary Sciences 15:47–72
1226 Schneider T, Bischoff T, Haug GH (2014) Migrations and dynamics of the
1227 intertropical convergence zone. Nature 513:45–53
1228 Shi G, Ribbe J, Cai W, Cowan T (2008) An interpretation of Australian rainfall
1229 projections. Geophysical Research Letters 35:L02702
1230 Shook KR, Pomeroy JW (2011) Memory effects of depressional storage in Northern
1231 Prairie hydrology. Hydrological Processes 25:3890–3898
1232 Shulmeister J (1992) A Holocene pollen record from lowland tropical Australia. The
1233 Holocene 2:107–116
1234 Shulmeister J, Lees BG (1995) Pollen evidence from tropical Australia for the onset
1235 of an ENSO-dominated climate at c. 4000 BP. The Holocene 5:10–18
1236 Siebers AR, Pettit NE, Skrzypek G, Fellman JB, Dogramaci S, Grierson PF (2015)
1237 Alluvial ground water influences dissolved organic matter biogeochemistry of
1238 pools within intermittent dryland streams. Freshwater Biology DOI:
1239 10.1111/fwb.12656
1240 Singarayer JS, Burrough SL (2015) Interhemispheric dynamics of the African rainbelt
1241 during the late Quaternary. Quaternary Science Reviews 124:48–67
1242 Skrzypek G (2013) Normalization procedures and reference material selection in
1243 stable HCNOS isotope analyses: an overview. Analytical and bioanalytical
1244 chemistry 405:2815–2823

1245 Skrzypek G, Dogramaci S, Grierson PF (2013) Geochemical and hydrological
1246 processes controlling groundwater salinity of a large inland wetland of
1247 northwest Australia. Chemical Geology 357:164–177
1248 Smith MA, Williams AN, Turney CSM, Cupper ML (2008) Human-environment
1249 interactions in Australian drylands: exploratory time-series analysis of
1250 archaeological records. The Holocene 18:389–401
1251 Smith MA, Ross J (2008) What happened at 1500-1000 cal. BP in Central Australia?
1252 Timing, impact and archaeological signatures. The Holocene 18:379–388
1253 Stager JC, Ryves DB, Chase BM, Pausata FSR (2011) Catastrophic drought in the
1254 Afro-Asian monsoon region during Heinrich event 1. Science 331:1299–1302
1255 Stager JC, Ryves DB, King C, Madson J, Hazzard M, Neumann FH, Maud R (2013)
1256 Late Holocene precipitation variability in the summer rainfall region of South
1257 Africa. Quaternary Science Reviews 67:105–120
1258 Stuut J-BW, Temmesfeld F, De D, Patrick (2014) A 550 ka record of aeolian activity
1259 near North West Cape, Australia: inferences from grain-size distributions and
1260 bulk chemistry of SE Indian Ocean deep-sea sediments. Quaternary Science
1261 Reviews 83:83–94
1262 Sutfin NA, Shaw JR, Wohl EE, Cooper DJ (2014) A geomorphic classification of
1263 ephemeral channels in a mountainous, arid region, southwestern Arizona, USA.
1264 Geomorphology 221:164–175
1265 Taschetto AS, England MH (2009) An analysis of late twentieth century trends in
1266 Australian rainfall. International Journal of Climatology 29:791–807
1267 Tierney JE, Oppo DW, Rosenthal Y, Russell JM, Linsley BK (2010) Coordinated
1268 hydrological regimes in the Indo-Pacific region during the past two millennia.
1269 Paleoceanography 25:PA1102

1270 Tierney JE, Smerdon JE, Anchukaitis KJ, Seager R (2013) Multidecadal variability in
1271 East African hydroclimate controlled by the Indian Ocean. Nature 493:389–392
1272 van der Kaars S, De Deckker P (2002) A Late Quaternary pollen record from deep-
1273 sea core Fr10/95, GC17 offshore Cape Range Peninsula, northwestern Western
1274 Australia. Review of Palaeobotany and Palynology 120:17–39
1275 van der Kaars S, De Deckker P, Gingele FX (2006) A 100 000-year record of annual
1276 and seasonal rainfall and temperature for north-western Australia based on a
1277 pollen record obtained offshore. Journal of Quaternary Science 21:879–889
1278 van Etten EJB (2009) Inter-annual Rainfall Variability of Arid Australia: greater than
1279 elsewhere? Australian Geographer 40:109–120
1280 Verschuren D (1999) Sedimentation controls on the preservation and time resolution
1281 of climate-proxy records from shallow fluctuating lakes. Quaternary Science
1282 Reviews 18:821–837
1283 Verschuren D (2004) Decadal and century-scale climate variability in tropical Africa
1284 during the past 2000 years. In: Battarbee RW, Gasse F, Stickley CE (eds) Past
1285 climate variability through Europe and Africa, Volume 6. Springer, Dordrecht,
1286 139–158
1287 Verschuren D, Charman DJ (2008) Latitudinal linkages in late Holocene moisture-
1288 balance variation. In: Battarbee RW, Binney HA (eds) Natural climate
1289 variability and global warming: a Holocene perspective. Wiley-Blackwell,
1290 Chichester, UK, 189–231
1291 Villalba R, Lara A, Masiokas MH, Urrutia R, Luckman BH, Marshall GJ, Mundo IA,
1292 Christie DA, Cook ER, Neukom R, others (2012) Unusual Southern Hemisphere
1293 tree growth patterns induced by changes in the Southern Annular Mode. Nature
1294 Geoscience 5:793–798

1295 Western Mail (1917) Our Flocks and Herds, 21 December 1917. Edition:
1296 CHRISTMAS, Trove (Perth, WA : 1885 - 1954). Available from:
1297 <http://nla.gov.au/nla.news-article37443627> [20 August 2014]
1298 Williams AN (2013) A new population curve for prehistoric Australia. Proceedings of
1299 the Royal Society B: Biological Sciences 280:389–401
1300 Williams AN, Veth P, Steffen W, Ulm S, Turney CSM, Reeves JM, Phipps SJ, Smith
1301 M (2015) A continental narrative: Human settlement patterns and Australian
1302 climate change over the last 35,000 years. Quaternary Science Reviews 123:91–
1303 112
1304 Woodborne S, Hall G, Robertson I, Patrut A, Rouault M, Loader NJ, Hofmeyr M
1305 (2015) A 1000-year carbon isotope rainfall proxy record from South African
1306 baobab trees (*Adansonia digitata* L.). PLoS ONE 10:e0124202
1307 Yan H, Sun L, Wang Y, Huang W, Qiu S, Yang C (2011) A record of the Southern
1308 Oscillation Index for the past 2,000 years from precipitation proxies. Nature
1309 Geoscience 4:611–614
1310 Yan H, Wei W, Soon W, An Z, Zhou W, Liu Z, Wang Y, Carter RM (2015)
1311 Dynamics of the intertropical convergence zone over the western Pacific during
1312 the Little Ice Age. Nature Geoscience 8:315–320
1313 Yancheva G, Nowaczyk NR, Mingram J, Dulski P, Schettler G, Negendank JFW, Liu
1314 J, Sigman DM, Peterson LC, Haug GH (2007) Influence of the intertropical
1315 convergence zone on the East Asian monsoon. Nature 445:74–77
1316

Table A.1: Results of AMS ^{14}C analyses used to derive the two age models. The unmodelled ages (*OxCal* v. 4.2; Bronk Ramsey, 2009) are provided in calibrated Common Era years (cal CE yrs); the two sigma (2σ) age range of the distributions with the highest probability density is provided. Results from bulk sediment were excluded from the age models due to the variable reservoir ages obtained. Sample depths of replicate core FOR106C2 were converted to FOR106C3 for calculations using visual layering of the sequences. Samples with the prefix 'OZ' and 'Wk-' were prepared and dated at ANSTO and the Waikato University, respectively.

Type	Core	Sample type	Lab ID	FOR106C3 Depth (cm)	FOR106C2 Depth (cm)	$\delta^{13}C$ (‰ VPDB)		pMC		^{14}C conv. age (BP)		Reservoir age (^{14}C yr)		Unmodelled age (cal CE yrs)		
								Mean	1σ	Mean	1σ	Mean	1σ	Median	2σ age range	
Macrofossils	FOR106C2	Terrestrial plant material	OZR585	8–9 [a]	8–9	−24.7		105.78	0.29	Modern				1957	1957	1958
														2009	2007	2011
	FOR106C2	Terrestrial plant material	OZQ883	19–20 [a]	18–19	−26.4		108.57	0.41	Modern				1958	1957	1959
														2002	2000	2004
	FOR106C3	Terrestrial plant material	OZQ887	23–24		−25.6		126.29	0.34	Modern				1962	1962	1963
														1981	1980	1982
	FOR106C3	Charred wood	OZQ888	31–32		−26.1		97.18	0.29	230	24			1757	1650	1954
	FOR106C3	Terrestrial plant seed	Wk–35517	35–36		−23.7		97.63	0.32	193	26			1768	1665	1955
	FOR106C3	Charred wood	OZQ891	39–40		−25.4		98.42	0.43	128	35			1855	1683	1955
	FOR106C2	Charred wood	OZR586	44–45 [a]	49–50	−25.0	[b]	84.64	0.79	1340	75			744	603	951
	FOR106C2	Charred wood	OZQ884	47–48 [a]	53–54	−25.0	[b]	85.36	0.86	1272	81			809	660	976
Bulk sediment	FOR106C3	Bulk sediment	OZQ886	23–24		−22.0		122.58	0.47	Modern		240	38			
	FOR106C3	Bulk sediment	OZQ889	35–36		−19.9		88.54	0.34	978	31	785	40			
	FOR106C3	Bulk sediment	OZQ890	39–40		−19.8		72.25	0.31	2611	34	2483	49			
	FOR106C3	Bulk sediment	OZQ892	53–54		−25.0	[b]	23.60	0.39	11600	140					
	FOR106C3	Bulk sediment	OZQ893	59–60		−25.0	[b]	23.63	0.32	11590	110					
	FOR106C2	Bulk sediment	OZQ885	60–61 [a]	64–65	−24.6		17.07	0.21	14200	100					

Note: [a] Equivalent FOR106C3 [b] Assumed $\delta^{13}C$ value as no measured $\delta^{13}C$ was available due to low carbon mass

Table A.2: Modelled ages provided in calibrated Common Era years (cal CE yrs) corresponding to AMS ^{14}C dated samples using Bayesian P_Sequence Model 1 (*OxCal* v. 4.2; Bronk Ramsey, 2009) and Smooth Spline Fitting Model 2 (*CLAM*; Blaauw, 2010), with respective 95% confidence intervals.

Depth (cm)	Modelled Age (cal CE yrs) - Model 1 *OxCal*			Modelled Age (cal CE yrs) - Model 2 *Clam*		
	Median	max95%	min95%	Best	max95%	min95%
8–9	2008	2007	2010	2005	1999	2009
18–19	1999	1987	2004	1986	1981	1992
23–24	1981	1962	1982	1980	1974	1987
31–32	1786	1742	1806	1908	1886	1922
35–36	1739	1694	1782	1778	1729	1821
39–40	1696	1672	1725	1548	1453	1645
49–50*	772	633	911	691	520	971
53–54*	672	533	839	335	120	683

Note: Depths corresponding to ages obtained from FOR106C2 have been provided as FOR106C3 equivalents
*Linearly extrapolated

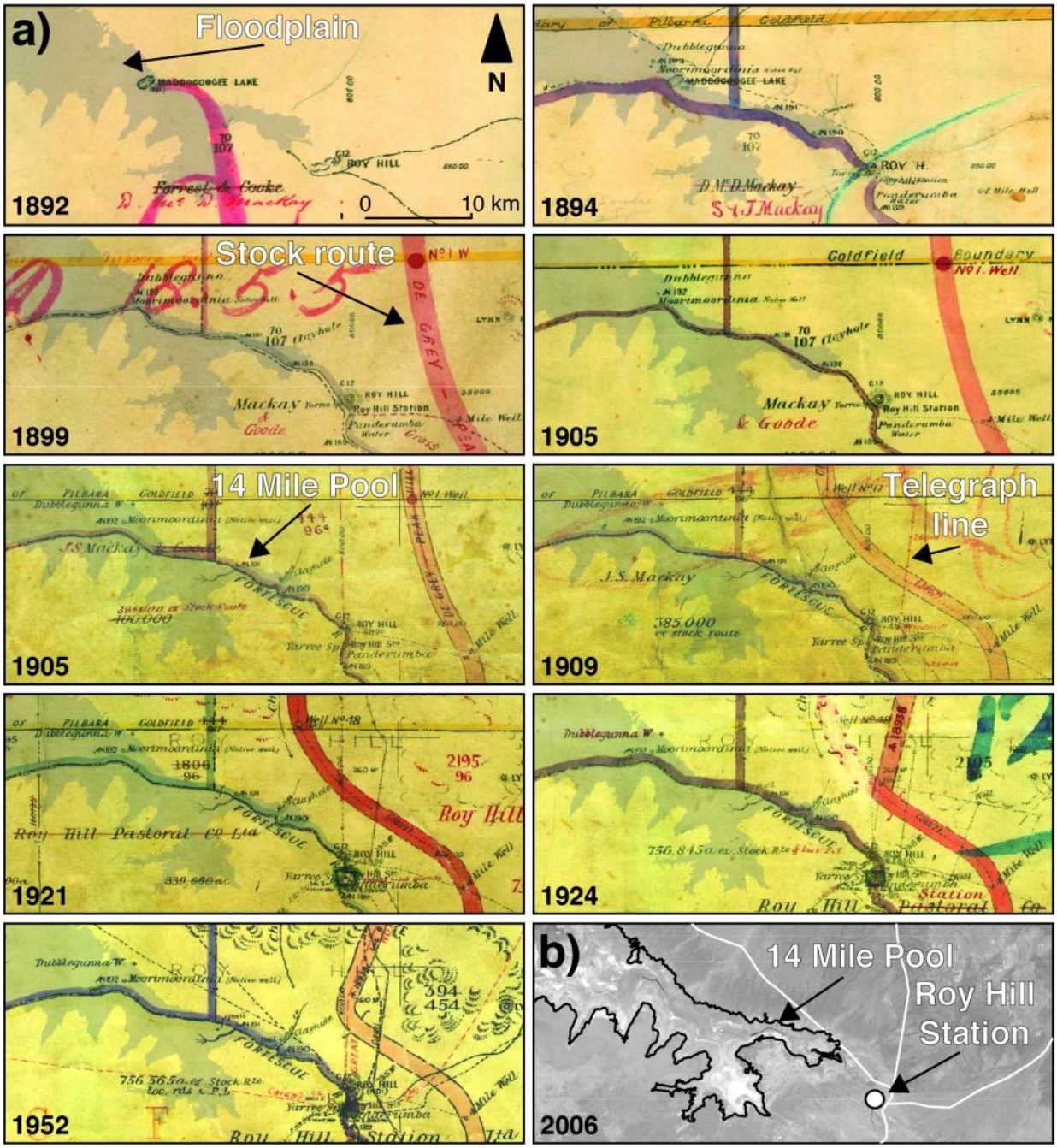

Figure A.1: Historical land use surrounding the 14 Mile Pool (1892–2010) from **a)** a public plans series ortho-rectified for the purpose of this study using landmarks (Dept Land and Surveys, 1892, 1894, 1899, 1905a,b, 1909, 1919, 1921, 1924, 1952) overlaid with the Fortescue Marsh floodplain (shaded blue area; modified from Chapter 2; USGS) and **b)** recent satellite image (Dec 2006; SPOT–5) showing the 14 Pool bed (darker linear shape), with the Fortescue Marsh floodplain (solid black line) and roads (solid white line).

2-COLUMN FITTING IMAGE